



ORIGINAL

Yasser Chiker · Mourad Bachene · Slim Bouaziz · Mouloud Guemana · Mounir Ben Amar · Mohamed Haddar

Free vibration analysis of hybrid laminated plates containing multilayer functionally graded carbon nanotube-reinforced composite plies using a layer-wise formulation

Received: 13 February 2020 / Accepted: 11 September 2020 / Published online: 24 September 2020
© Springer-Verlag GmbH Germany, part of Springer Nature 2020

Abstract This paper studies the free vibration behavior of hybrid laminated plates using a layer-wise formulation. The laminated structures are made of graphite fiber-reinforced composite (GFRC) and multilayer functionally graded carbon nanotube-reinforced composite (FG-CNTRC) plies. The internal single-walled carbon nanotubes (SWCNTs) are distributed in layer-wise form along the ply thickness direction either uniformly or functionally graded according to four separate patterns. Both the linear and nonlinear of the CNTs distributions form are considered. Theoretical formulations are based on the first-order shear deformation theory (FSDT), and finite element method is employed to obtain the nondimensional natural frequency. The elastic modulus of both GFRC and CNTRC plies composed the hybrid laminated plate is obtained by a micromechanics model. Initially, the provided results are validated by comparing it with the literature; thereafter, a parametric study is carried out the influences of laminates configuration, number of CNTRC plies layers, CNT volume fraction, CNT distribution patterns, linear and nonlinear distribution of CNTs, plate width-to-thickness ratio, plate aspect ratio, boundary conditions, stacking sequences, and number of plies on the free vibration behavior of hybrid laminated plates. Some final remarks considering the laminated plate configuration and the distribution form of the CNT fillers are presented in order to provide a useful observation on the design criteria of the laminated composite plate structures.

Keywords Free vibration · Hybrid laminated plate · Functionally graded · Graphite · Carbon nanotube · First-order shear deformation theory

1 Introduction

Due to their extremely attractive thermal, mechanical, and electrical properties, carbon nanotubes (CNTs) have been progressively introduced as an excellent reinforcement for composite materials instead of ordinary fibers [1–5]. The combination of a polymer matrix and CNTs or in other words carbon nanotube-reinforced

Y. Chiker (✉) · M. Bachene
Laboratory of Mechanics, Physics, Mathematical Modeling (LMP2M), University of Medea, Medea, Algeria
E-mail: chiker.yasser@univ-medea.dz

S. Bouaziz · M. Haddar
Mechanics, Modelling and Production Laboratory (LA2MP), National engineering School of Sfax, University of Sfax, Sfax, Tunisia

M. Guemana
Laboratory of Applied Automation and Industrial Diagnostic (LAADI), University of Djelfa, Djelfa, Algeria

M. B. Amar
Laboratoire des Sciences des Procédés et des Matériaux, CNRS, Université Paris 13, Villetaneuse, France

composite (CNTRC), leads the nanocomposites structures to have high stiffness and high strength with a lighter weight of about four times compared to the metal material structures [6,7]. Owing to these excellent properties, many researchers considered CNTs to be an outstanding reinforcement for advanced performance composite [8–10]. Qian et al. [11] revealed that only 1 % of CNTs weight fraction is able to enhance the mechanical properties of the polystyrene carbon nanotube-reinforced composite by 36–42%. Moreover, it has been noted from many published papers that dispersing the CNTs in a nonuniform way through the thickness direction can considerably enhance the mechanical behavior of the nanocomposite structures. A literature review on the recent progress of functionally graded carbon nanotube (FG-CNT)-reinforced composites and structures was reported recently by Liew et al. [12].

Inspired by the concept of functionally graded materials (FGMs) [13–17], Shen examined the carbon nanotubes successfully in terms of functionally graded dispersion in a polymer matrix across the thickness direction [18]. Recently, many researchers in diverse field such as science and engineering give great interest in the functionally graded CNTRC concept, as this interest has been translated into several publications over the past few years, with the aim of studying many influencing parameters, including CNT volume fraction and CNT distribution patterns for static analysis [19], forced vibration analysis [20,21], free vibration analysis [22–24], buckling analysis [25–27], and postbuckling analysis [28,29]. Owing to its geometrical shape, composite plate structures are very essential structural components, and they support various external forces applied to them with all efficiency and effectiveness. The plates structures are extensively used in diverse fields such as marine, civil, architectural, and aeronautical engineering, they are often subjected to varying dynamic loads that produce vibrations, so investigate the vibration behavior of those structures is an essential task for a successful application. Many investigations are reported to study the vibration behavior of CNTRC square plate [30], skew plates [31,32], triangular plates [33], quadrilateral plates [34,35], arbitrarily shaped plates [36], sandwich plates [37], and laminated plates [38].

Composite laminated plate structures are largely used in several structural applications due to their high mechanical performance compared to a single-layer structure. In this regard, numerous work has been carried the performance of CNTRC laminated plates. Based on the first-order shear deformation theory Lei et al. [39] investigated the bending responses of perfectly bonded FG-CNT-reinforced composite plates using the element-free kp-Ritz method. Based on the same approach Lei et al. [40] studied the buckling behavior of FG-CNT-reinforced composite laminated plate using the meshless kp-Ritz method. Shen and Xiang [41] employed the Reddy's third-order shear deformation shell theory including the effects of the temperature change to examine the postbuckling behavior of the FG graphene platelet-reinforced composite laminated cylindrical shells subjected to thermo-mechanical load using an analytical approach. Employing the element-free kp-Ritz method, Lei et al. [42] analyzed the vibration behavior of perfectly bonded rotating laminated cylindrical panels with FG-CNT-reinforced composite layers. Malekzadeh and Zarei [43] employed the FSDT to study the free vibration characteristics of thin-to-moderately thick quadrilateral laminated plates with CNTRC layers. The authors concluded that, for both thin and moderately thick plate, the distribution of CNTs across the thickness direction corresponding to FG-X patterns leads to a stiffer composite plate then in comparison with other distribution patterns. Using a semi-analytical approach Malekzadeh and Heydarpour [44] presented the static and three-dimensional free vibration analysis of perfectly bonded laminated plates with FG-CNT-reinforced composite layers. Studying two different sandwich plates models, the authors found that the stiffness of the laminated plate affected by the plate configuration. Employing the FSDT Lei et al. [38] investigated the vibration behavior of perfectly bonded thin-to-moderately thick laminated FG-CNT-reinforced composite rectangular plates, the effect of CNT distributions patterns, CNT volume fraction, number of plate layers, and geometrical parameters were discussed. Employing a simple four-variable FSDT, Huang et al. [45] studied the free vibration and bending problems of antisymmetrically laminated FG-CNT-reinforced composite plates. The authors concluded that each of CNT volume fraction, CNT distribution types, number of layer, and geometrical parameters have a remarkable influence on the dynamic characterizations of CNTRC laminated plates.

Moreover, Fan and Wang [46] investigated the large amplitude vibration and thermal postbuckling of thermally postbuckled hybrid laminated plates containing conventional fibers and FG-CNT layers. Lei et al. [47] presented a mathematical model for nonlinear vibration analysis of a hybrid laminated plate composed of CNTRC layers and GFRC layers. In their investigation, the different distribution types of CNTs, matrix cracks density, CNT volume fraction, number of layers, and geometry parameters were considered. Lei et al. [48] studied the banding and vibration behavior of both cracked and un-cracked hybrid laminated plates containing graphite fiber-reinforced composite layers and FG-CNT-reinforced composite layers. The authors presented a detailed parametric study to investigate the influence of material parameters, boundary condition, and geometrical parameters on banding and vibration responses of the laminated hybrid plate. Using the FSDT,

Pan et al. [49] proposed a model for geometrically nonlinear large deformation behaviors of matrix cracked hybrid composite double-curved deep shell composed of graphite fiber-reinforced composite layers and FG-CNT-reinforced composite layers. Comparing the two models of sandwich plates the authors concluded that for the design process it is important to take into consideration crack influence in the matrix for the nonlinear deflection response. In addition, comparing between two plate structure types the authors found that the laminated shell configuration can improve the resisting of deformation under external loadings.

The present paper aims to study the free vibration behavior of hybrid laminated plates that contain multilayer CNTRC and GFRC plies, with multiple plate configuration employing a layer-wise formulation. The FSDT is employed to characterize the displacement fields in the hybrid composite plate. The elastic modulus of both GFRC and CNTRC plies is estimated based on micromechanics model. The parametric investigations are examined to exhibit the effect of plate configuration, CNT volume fraction, CNT destruction patterns, linear and nonlinear distribution of CNTs, number of CNTRC ply' layers, boundary condition, and the number of plate' plies on the free vibration behavior of hybrid laminated plate.

2 Problem formulation

2.1 Geometrical and CNT distribution pattern characterization

A perfectly bonded hybrid laminated plate with length (a), width (b), and total thickness (h) is taken under consideration in the current study. The hybrid laminated plate is defined in a three-dimensional coordinate system (x, y, z) in which x -, y -, and z -axes are, respectively, parallel to the length, width, and thickness direction, as depicted in Fig. 1a. It is assumed that the hybrid laminated plates consist of (P_t) plies in which each ply is either made of CNTRC or GFRC. The CNTRC plies are divided into (N_L) layers in which each layer has the same thickness ($\Delta h = t/N_L$) where t is the CNTRC ply thickness. It is assumed that each individual layer of the CNTRC plies has a uniform dispersion of CNT fillers in the plane (x, y) embedded in a polymer matrix and a different amount of it from layer to layer across the ply thickness. So far, five different distributions patterns, denoted by UD, FG-V, FG- Λ , FG-O, and FG-X are considered in the present study as depicted in Fig. 1b. The CNT volume fraction shows a layer-wise change in order to shape the functionally graded structure; accordingly, the CNT volume fraction of the k th CNTRC ply' layer ($f_{\text{CNT}}^{(k)}$) for the five CNT distribution patterns is given as follows [50]:

$$\text{UD} : f_{\text{CNT}}^{(k)} = f_{\text{CNT}}^* \quad (1)$$

$$\text{FG-V} : f_{\text{CNT}}^{(k)} = f_{\text{CNT}}^* (P_{\text{in}} + 1) \left(\frac{k - 0.5}{N_L} \right)^{P_{\text{in}}} \quad (2)$$

$$\text{FG-}\Lambda : f_{\text{CNT}}^{(k)} = f_{\text{CNT}}^* (P_{\text{in}} + 1) \left(\frac{0.5 - k + N_L}{N_L} \right)^{P_{\text{in}}} \quad (3)$$

$$\text{FG-O} : f_{\text{CNT}}^{(k)} = f_{\text{CNT}}^* (P_{\text{in}} + 1) \left(\frac{1 - |2k - N_L - 1|}{N_L} \right)^{P_{\text{in}}} \quad (4)$$

$$\text{FG-X} : f_{\text{CNT}}^{(k)} = f_{\text{CNT}}^* (P_{\text{in}} + 1) \left(\frac{|2k - N_L - 1|}{N_L} \right)^{P_{\text{in}}} \quad (5)$$

in which $k = 1, 2, 3 \dots N_L$, P_{in} denote the power-law index or (the index that controls the distribution form of the CNT fillers) and f_{CNT}^* is the total volume fraction, which is given as follows:

$$f_{\text{CNT}}^* = \frac{w_{\text{CNT}}}{w_{\text{CNT}} + (\rho^{\text{CNT}}/\rho^m)(1 - w_{\text{CNT}})} \quad (6)$$

where w_{CNT} is the mass fraction of CNTs; and ρ^{CNT} and ρ^m denote, respectively, the mass density of the CNT fillers and polymer matrix. It should be noted that for all five distribution patterns the total volume fraction is the same.

Figure 2 shows the variation of the CNT volume fraction ratio ($f_{\text{CNT}}^{(k)}/f_{\text{CNT}}^*$) along the thickness direction of a single ply of CNTRC plate with different CNT distribution patterns and power-law indexes. As can be seen the plates with UD pattern represent a special case, where the CNT fillers are distributed homogeneously

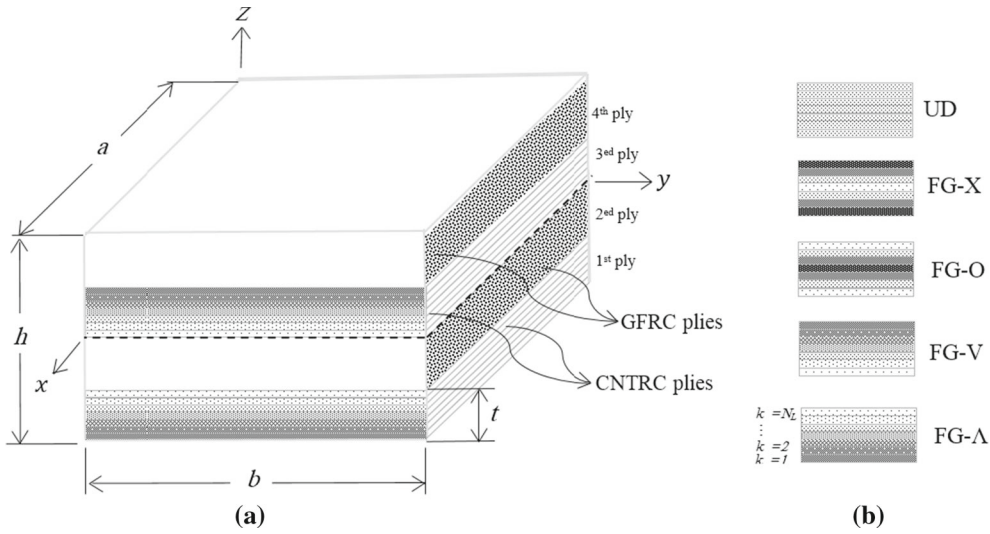


Fig. 1 a Coordinate system and geometry of perfectly bounded hybrid laminated plate composed of GFRC and CNTRC plies; b different distribution types of the CNT fillers

across the thickness direction of the plate, which leads to an unchanged $f_{CNT}^{(k)} / f_{CNT}^*$ for all values of z/h . As for the nonuniform distribution types, which are FG- Δ , FG-V, FG-O, and FG-X patterns the CNT fillers dispersed in linear ($P_{in} = 1$) and nonlinear ($P_{in} = 0.4, 0.8, 1.4, \text{ and } 1.8$) form, respectively, either from the plate's bottom surface to the top, from the plate's top surface to the bottom, from the mid-plane of the plate to the top, and bottom surfaces or from the top and bottom surfaces to the mid-plane of the plate. In addition, one can see that the CNT volume fraction ratios $f_{CNT}^{(k)} / f_{CNT}^*$ change in a symmetrical way for the plates with UD, FG-O, and FG-X patterns and unsymmetrical way for the plates with FG-V and FG- Δ patterns.

It is noteworthy that the combined plates are named by meeting the letter of the CNT distribution type denoted by ($\Delta, V, O, X,$ and UD) or GFRC denoted by (F) of each ply. For example, the laminate configuration shown in Fig. 1 [Δ -F-V-F], means that the first ply from the bottom surface of the laminated plate to the top has FG- Δ distribution pattern, the second ply is made with GFRC, the third ply is made with FG-V distribution pattern, and the fourth ply is made with GFRC.

Since the under consideration composite hybrid laminated plates contain plies of CNTRC and GFRC, in the following, we will consider two different micromechanics models to describe the mechanical properties of each of these two compounds.

2.2 Mechanical priorities of the GFRC plies

Employing the micromechanical model, the material properties of GFRC plies can be expressed as [51]:

$$E_{11} = f_F E_{11}^F + f_m E^m \tag{7}$$

$$\frac{1}{E_{22}} = \frac{f_F}{E_{22}^F} + \frac{f_m}{E^m} - f_F f_m \frac{f_F^2 E^m / E_{22}^F + f_m^2 E_{22}^F / E^m - 2\nu^F \nu^m}{f_F E_{22}^F + f_m E^m} \tag{8}$$

$$\frac{1}{G_{12}} = \frac{f_F}{G_{12}^F} + \frac{f_m}{G^m} \tag{9}$$

$$\rho = f_F \rho^F + f_m \rho^m \tag{10}$$

$$\nu_{12} = f_F \nu^F + f_m \nu^m \tag{11}$$

where E , G , and ν are, respectively, Young's modulus, shear modulus, and Poisson's ratio.

And (m) denotes matrix, while (F) denotes graphite fiber.

Related by the following relationship $f_m + f_F = 1$, f_m and f_F are, respectively, the volume fractions of the matrix and graphite fibers.

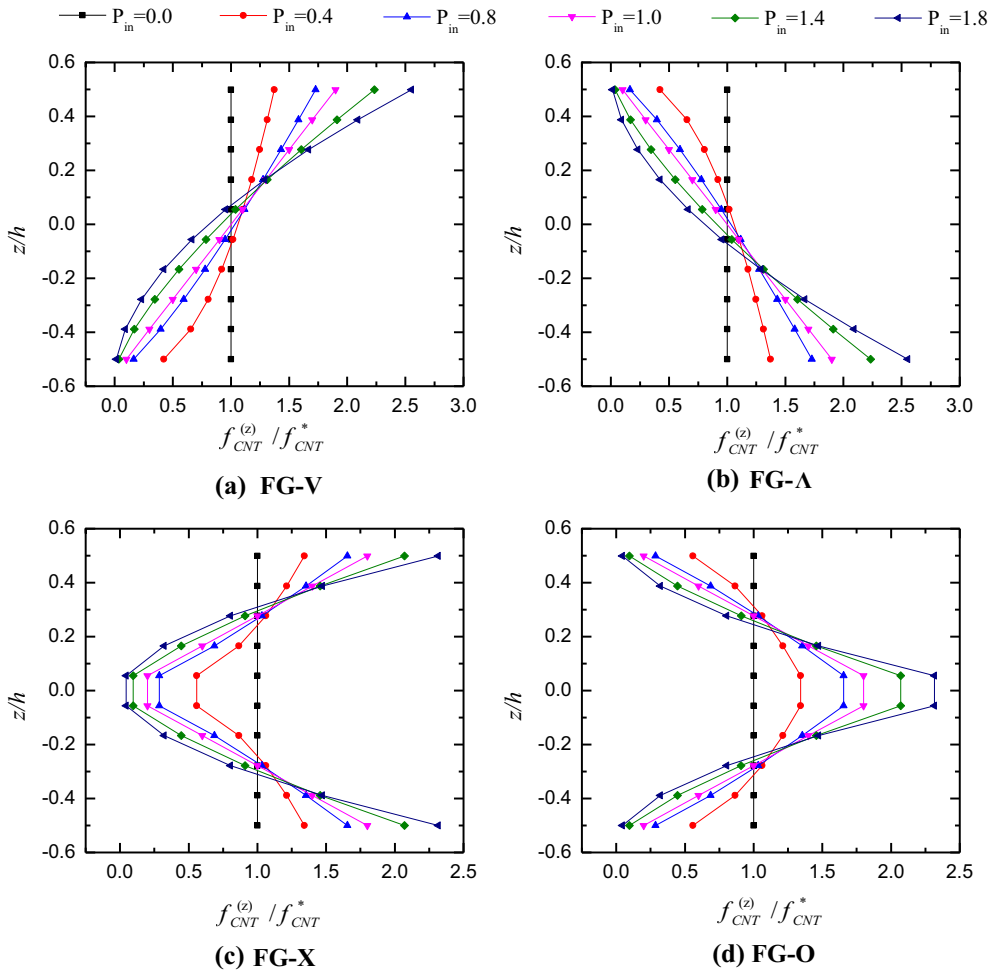


Fig. 2 Variation of the CNT volume fraction ratio ($f_{CNT}^{(z)} / f_{CNT}^*$) across the CNTRC plate thickness for different CNT distribution patterns

3 Mechanical properties of the CNTRC plies

According to the extended rule of mixture [52] the effective proprieties of the k th CNTRC ply' layer are given by [18]:

$$E_{11}^{(k)} = \eta_1 f_{CNT}^{(k)} E_{11}^{CNT} + f_m^{(k)} E_m \tag{12}$$

$$\frac{\eta_2}{E_{22}^{(k)}} = \frac{f_{CNT}^{(k)}}{E_{22}^{CNT}} + \frac{f_m^{(k)}}{E_m} \tag{13}$$

$$\frac{\eta_3}{G_{12}^{(k)}} = \frac{f_{CNT}^{(k)}}{G_{12}^{CNT}} + \frac{f_m^{(k)}}{G_m} \tag{14}$$

$$\nu_{12}^{(k)} = f_{CNT}^{(k)} \nu_{12}^{CNT} + f_m^{(k)} \nu_m \tag{15}$$

$$\rho^{(k)} = f_{CNT}^{(k)} \rho^{CNT} + f_m^{(k)} \rho_m \tag{16}$$

where (m) and (CNT) denote, respectively, the polymer matrix and carbon nanotubes. The parameter η_j ($j = 1, 2, 3$) represents the CNT efficiency parameters, which are used in order to deal with the small-scale effect [18]. Related by $f_{CNT} + f_m = 1$, f_m and f_{CNT} are, respectively, the volume fraction of the matrix and the CNT.

3.1 Governing equations for laminated plate

Based on the first-order shear deformation plate theory FSDT [53] the displacement field at an arbitrary point $M(x, y, z)$ in the ply is expressed as follows:

$$\begin{aligned} u(x, y, z) &= u_0(x, y) + z\theta_x(x, y) \\ v(x, y, z) &= v_0(x, y) + z\theta_y(x, y) \\ w(x, y, z) &= w_0(x, y) \end{aligned} \quad (17)$$

where $u_0(x, y)$, $v_0(x, y)$, and $w_0(x, y)$ denote the displacements component of a point on the mid-plane of the ply and θ_x, θ_y are, respectively, the rotations of the cross section of the ply about y - and x -axes.

According to the FSDT, the strain–displacement relations are expressed as follows:

$$\begin{Bmatrix} \varepsilon_x \\ \varepsilon_y \\ \varepsilon_{xy} \end{Bmatrix} = \begin{Bmatrix} \varepsilon_x^{(0)} \\ \varepsilon_y^{(0)} \\ \gamma_{xy}^{(0)} \end{Bmatrix} + z \begin{Bmatrix} \varepsilon_x^{(1)} \\ \varepsilon_y^{(1)} \\ \gamma_{xy}^{(1)} \end{Bmatrix}, \quad \begin{Bmatrix} \gamma_{yz} \\ \gamma_{xz} \end{Bmatrix} = \gamma^{(0)} \quad (18)$$

where

$$\begin{Bmatrix} \varepsilon_x^{(0)} \\ \varepsilon_y^{(0)} \\ \gamma_{xy}^{(0)} \end{Bmatrix} = \begin{Bmatrix} \frac{\partial u_0}{\partial x} \\ \frac{\partial v_0}{\partial y} \\ \frac{\partial u_0}{\partial y} + \frac{\partial v_0}{\partial x} \end{Bmatrix}, \quad \begin{Bmatrix} \varepsilon_x^{(1)} \\ \varepsilon_y^{(1)} \\ \gamma_{xy}^{(1)} \end{Bmatrix} = \begin{Bmatrix} \frac{\partial \theta_x}{\partial x} \\ \frac{\partial \theta_y}{\partial y} \\ \frac{\partial \theta_x}{\partial y} + \frac{\partial \theta_y}{\partial x} \end{Bmatrix}, \quad \gamma^{(0)} = \begin{Bmatrix} \frac{\partial w_0}{\partial y} + \theta_y \\ \frac{\partial w_0}{\partial x} + \theta_x \end{Bmatrix} \quad (19)$$

Then, the stress–strain constitutive relations of the ply can be expressed as:

$$\begin{Bmatrix} \sigma_x \\ \sigma_y \\ \sigma_{xy} \\ \sigma_{yz} \\ \sigma_{xz} \end{Bmatrix} = \begin{bmatrix} Q_{11} & Q_{12} & 0 & 0 & 0 \\ Q_{12} & Q_{22} & 0 & 0 & 0 \\ 0 & 0 & Q_{44} & 0 & 0 \\ 0 & 0 & 0 & Q_{55} & 0 \\ 0 & 0 & 0 & 0 & Q_{66} \end{bmatrix} \begin{Bmatrix} \varepsilon_x \\ \varepsilon_y \\ \gamma_{xy} \\ \gamma_{yz} \\ \gamma_{xz} \end{Bmatrix} \quad (20)$$

where

$$Q_{11} = \frac{E_{11}}{1 - \nu_{12}\nu_{21}}, \quad Q_{12} = \frac{\nu_{21}E_{11}}{1 - \nu_{12}\nu_{21}}, \quad Q_{22} = \frac{E_{22}}{1 - \nu_{12}\nu_{21}}, \quad Q_{66} = G_{13}, \quad Q_{55} = G_{23}, \quad Q_{44} = G_{12}, \quad (21)$$

The strains–stress relationships are defined as:

$$\begin{Bmatrix} N_x \\ N_y \\ N_{xy} \end{Bmatrix} = [A] \begin{Bmatrix} \varepsilon_x^{(0)} \\ \varepsilon_y^{(0)} \\ \gamma_{xy}^{(0)} \end{Bmatrix} + [B] \begin{Bmatrix} \varepsilon_x^{(1)} \\ \varepsilon_y^{(1)} \\ \gamma_{xy}^{(1)} \end{Bmatrix}, \quad (22)$$

$$\begin{Bmatrix} M_x \\ M_y \\ M_{xy} \end{Bmatrix} = [B] \begin{Bmatrix} \varepsilon_x^{(0)} \\ \varepsilon_y^{(0)} \\ \gamma_{xy}^{(0)} \end{Bmatrix} + [D] \begin{Bmatrix} \varepsilon_x^{(1)} \\ \varepsilon_y^{(1)} \\ \gamma_{xy}^{(1)} \end{Bmatrix}, \quad (23)$$

$$\begin{Bmatrix} Q_y \\ Q_x \end{Bmatrix} = k_s [F] \begin{Bmatrix} \gamma_{yz} \\ \gamma_{xz} \end{Bmatrix}, \quad (24)$$

where

N , M , and Q are respectively the total in plane forces, moment resultants and shear forces, taken to be $5/6$, k_s is the shear correction coefficient.

And

A_{ij} , B_{ij} , D_{ij} , and F_{ij} are the stiffness elements given as:

$$(A_{ij}, B_{ij}, D_{ij}) = \sum_{k=1}^{P_l} \int_{z_k}^{z_{k+1}} Q_{ij}^{(k)}(1, z, z^2) dz, \quad (i, j = 1, 2, 6) \quad (25)$$

$$F_{ij} = k_s \sum_{k=1}^{P_t} \int_{z_k}^{z_{k+1}} Q_{ij}^{(k)} dz, \quad (ij = 4, 5) \quad (26)$$

$$= k_s \sum_{k=1}^{P_t} \int_{z_k}^{z_{k+1}} Q_{ij}^{(k)} dz, \quad (j = 4, 5) \quad (27)$$

3.2 Finite element formulation

A nine-noded isoperimetric element based on the Mindlin–Reissner plate theory was employed in the current study. It is noteworthy that the approach takes into consideration the effect of transverse shear deformation. Each node of the element has five degrees of freedom ($u_i, v_i, w_i, \theta_{yi}, \theta_{xi}$), and the generalized displacement through the element can be expressed as:

$$u_0 = \sum_{i=1}^9 N_i u_{0i}, \quad v_0 = \sum_{i=1}^9 N_i v_{0i}, \quad w_0 = \sum_{i=1}^9 N_i w_{0i}, \quad \theta_x = \sum_{i=1}^9 N_i \theta_{xi}, \quad \theta_y = \sum_{i=1}^9 N_i \theta_{yi} \quad (28)$$

where N_i is the shape function

Based on the standard finite element procedure the governing equations for the free vibration of the hybrid laminated plate take the following form [54]:

$$K \delta + M \ddot{\delta} = 0 \quad (29)$$

where K denotes the stiffness matrix and M is the mass matrix, $\ddot{\delta}$ and δ are, respectively, the global acceleration and displacement vectors,
and

$$[k_e] = \int_{\Lambda_e} [B]^T [C] [B] d\Lambda_e \quad (30)$$

$$[M_e] = \int_{\Lambda_e} [N]^T [\bar{m}] [N] d\Lambda_e \quad (31)$$

where

$$C = \begin{bmatrix} A & B & 0 \\ B & D & 0 \\ 0 & 0 & F \end{bmatrix}, \quad \bar{m} = \begin{bmatrix} I_0 & 0 & 0 & I_1 & 0 \\ 0 & I_0 & 0 & 0 & I_1 \\ 0 & 0 & I_0 & 0 & 0 \\ I_1 & 0 & 0 & I_2 & 0 \\ 0 & I_1 & 0 & 0 & I_2 \end{bmatrix} \quad (32)$$

$$[B_i] = \begin{bmatrix} \frac{\partial N_i}{\partial x} & 0 & 0 & 0 & 0 \\ 0 & \frac{\partial N_i}{\partial y} & 0 & 0 & 0 \\ \frac{\partial N_i}{\partial y} & \frac{\partial N_i}{\partial y} & 0 & 0 & 0 \\ 0 & 0 & 0 & \frac{\partial N_i}{\partial x} & 0 \\ 0 & 0 & 0 & 0 & \frac{\partial N_i}{\partial y} \\ 0 & 0 & 0 & \frac{\partial N_i}{\partial x} & \frac{\partial N_i}{\partial x} \\ 0 & 0 & \frac{\partial N_i}{\partial x} & N_i & 0 \\ 0 & 0 & \frac{\partial N_i}{\partial y} & 0 & N_i \end{bmatrix} \quad (33)$$

in which Λ_e is the elementary surface, and C, \bar{m}, B are, respectively, the elasticity, the inertia, and the strain interpolation matrices.

The inertia-associated terms are defined by:

$$I_i = \sum_{k=1}^{P_l} \int_{z_k}^{z_{k+1}} z^i \rho^{(k)} dz, \quad (i = 0, 1, 2) \tag{34}$$

Assuming that the composite plate undergoes a harmonic motion (given that we dealing with a free vibration analysis), Eq. (29) turns into a generalized eigenvalue problem, where the dynamic properties, frequencies (ω), and mode shapes ($\bar{\delta}$) can be obtained by solving the following relation:

$$(K - \omega^2 M)\bar{\delta} = 0 \tag{35}$$

The following homogeneous boundary conditions (BCs) are employed to analyze the present investigation:

I. Simply supported edge (S):

- Cross-ply laminate:

At $x = 0, a: v_0 = w_0 = \theta_y = 0$.
 At $y = 0, b: u_0 = w_0 = \theta_x = 0$.

- Angle-ply laminate:

At $x = 0, a: u_0 = w_0 = \theta_y = 0$,
 At $y = 0, b: v_0 = w_0 = \theta_x = 0$.

II. Clamped edge (C):

On all edges $u_0 = v_0 = w_0 = \theta_x = \theta_y = 0$, for both cross-ply and angle-ply laminate.

4 Numerical results and discussion

A detailed parametric analysis is conducted to study the effect of the laminated plate configuration and the CNT fillers distribution form on the free vibration behavior of hybrid laminated plates. In the **current** study, different level of CNT volume fraction, power-law index, geometry parameter, as well as plates stacking sequence, boundary conditions and ply' number, are taken into account as a parameter under investigation. Before performing the numerical examples, it is required to determine the material properties of both CNTRC and GFRC plies. It is assumed that the poly(m-phenylenevinylene)-co-[(2,5-dioctoxy-p-phenylene) vinylene] (PmPV) polymer is chosen as a matrix for both CNTRC and GFRC plies, and the properties of the polymer matrix are taken to be $E^m = 2.1\text{GPa}$, $\nu^m = 0.34$, $\rho^m = 1150\text{kg/m}^3$. As a reinforcement in the CNTRC plies, the (10, 10) single-walled carbon nanotubes (SWCNTs) are chosen, whose properties are: $E_{11}^{\text{CNT}} = 5646.6\text{GPa}$, $E_{22}^{\text{CNT}} =$

Table 1 Comparisons of the fundamental nondimensional frequency ($\bar{\omega} = \omega\sqrt{\rho_c/E_c}$) of SSSS AL/AL₂O₃ FGM plate with different power-law index, width-to-thickness ratio, and mesh sizes

b/h	Source	P_{in}				
		0.0	0.5	1.0	4.0	10.0
05	Present 4×4	0.2111	0.1811	0.1630	0.1388	0.1306
	Present 6×6	0.2112	0.1812	0.1631	0.1389	0.1307
	Present 8×8	0.2112	0.1812	0.1631	0.1389	0.1308
	Present 12×12	0.2112	0.1812	0.1631	0.1389	0.1308
	Matsunaga [55]	0.2121	0.1819	0.1640	0.1383	0.1306
10	Song et al. [56]	0.2112	0.1809	0.1634	0.1393	0.1316
	Present 4×4	0.05767	0.04921	0.04423	0.03804	0.03611
	Present 6×6	0.05769	0.04923	0.04424	0.03805	0.03613
	Present 8×8	0.05769	0.04923	0.04425	0.03805	0.03613
	Present 12×12	0.05769	0.04923	0.04425	0.03805	0.03613
	Matsunaga [55]	0.05777	0.04917	0.04426	0.03811	0.03642
	Song et al. [56]	0.05769	0.04912	0.04427	0.03811	0.03632

Table 2 Comparisons of the first six nondimensional frequency ($\bar{\omega} = \omega(b^2/h)\sqrt{\rho^m/E^m}$) of cross-ply ($0^0/90^0/0^0/90^0/0^0$) laminated CNTRC plates with two type of boundary conditions for $a/b = 1$, $b/h = 10$, $N_L = 20$ and $f_{CNT}^* = 0.11$

BCs	FG-O		FG-V		UD		FG-X	
	Present	Reference [38]	Present	Reference [38]	Present	Reference [38]	Present	Reference [38]
SSSS	14.096	14.207	14.118	14.241	14.17	14.277	14.276	14.383
	19.257	19.463	19.253	19.463	19.208	19.414	19.257	19.463
	19.257	19.468	19.253	19.468	19.208	19.419	19.257	19.468
	26.497	26.955	26.536	27.026	26.654	27.098	26.882	27.318
	30.278	30.578	30.276	30.602	30.288	30.579	30.415	30.704
	37.048	38.240	37.016	38.296	36.956	38.312	37.05	38.526
CCCC	19.737	19.652	19.758	19.678	19.771	19.680	19.878	19.784
	30.666	30.862	30.681	30.902	30.722	30.906	30.895	31.074
	32.672	32.752	32.678	32.773	32.664	32.736	32.794	32.862
	39.848	40.549	39.839	40.585	39.868	40.554	40.051	40.732
	45.361	46.270	45.369	46.324	45.407	46.315	45.639	46.552
	48.13	49.277	48.128	49.294	48.071	49.209	48.231	49.369

Table 3 Comparisons of the fundamental nondimensional frequency ($\bar{\omega} = \omega(b^2/h)\sqrt{\rho^m/E^m}$) of cross-ply ($0^0/90^0$)_n and angle-ply ($45^0/-45^0$)_n laminated CNTRC plates with different number of lyres for $a/b=1$, $b/h=50$, $N_L = 20$, and $f_{CNT}^* = 0.11$

Stacking sequences	n	FG-O		FG-V		UD		FG-X	
		Present	Reference [45]	Present	Reference [45]	Present	Ref [45]	Present	Reference [45]
$(0^0/90^0)$	1	09.156	9.182	10.134	10.056	11.341	11.348	13.092	13.064
	2	17.495	17.378	17.51	17.495	17.688	17.714	17.985	17.975
	4	18.883	18.856	18.884	18.883	18.922	18.958	18.995	18.995
$(45^0/-45^0)$	1	12.116	11.974	13.189	14.116	15.094	15.109	17.653	17.697
	2	23.946	23.761	23.87	23.946	24.134	24.180	24.55	24.601
	4	25.871	25.818	25.793	25.871	25.85	25.912	25.951	26.012

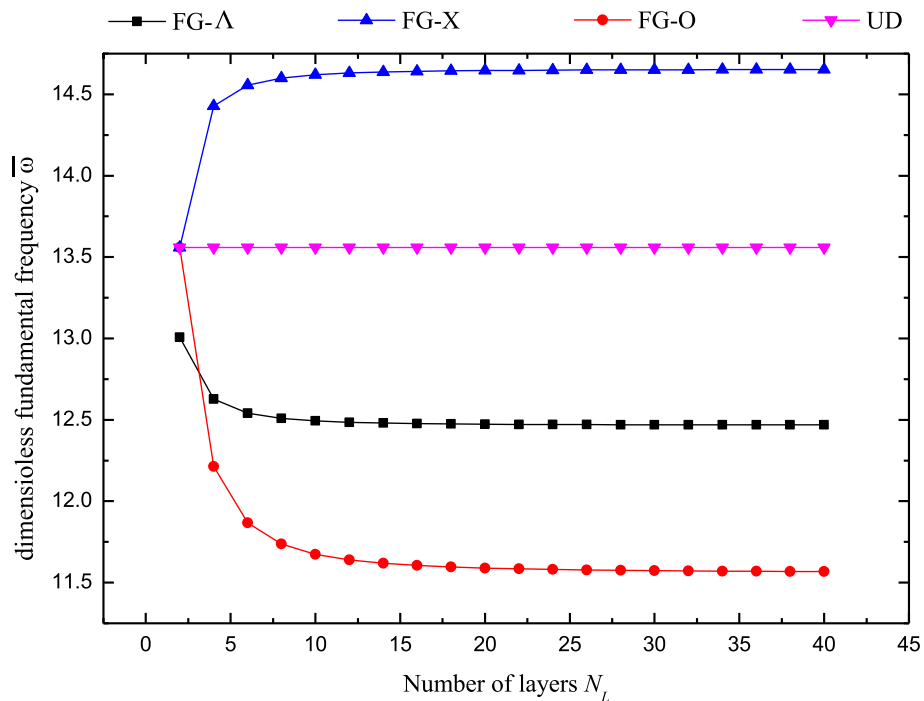


Fig. 3 Effect of number of layers on the nondimensional frequency $\bar{\omega} = \omega(b^2/h)\sqrt{\rho^m/E^m}$ for single ply of CNTRC plate

Table 4 Fundamental nondimensional frequency ($\bar{\omega} = \omega(b^2/h)\sqrt{\rho^m/E^m}$) of cross-ply $(0^C/90^F)_n$ hybrid laminated composite plates with various values of CNT volume fraction ($a/b = 1, b/h = 10$)

	f_{CNT}^*	SSSS				CCCC			
		[UD - F] _n	[Λ - F] _n	[O - F] _n	[X - F] _n	[UD - F] _n	[Λ - F] _n	[O - F] _n	[X - F] _n
$n = 1$	0.11	11.442	11.384	10.796	12.027	20.511	20.393	19.520	21.295
	0.14	11.804	11.750	11.021	12.502	21.028	19.954	19.898	21.890
	0.17	12.493	12.437	11.600	13.297	22.285	21.933	20.996	23.281
$n = 2$	0.11	15.939	15.874	15.853	16.032	25.292	25.266	25.211	25.392
	0.14	16.566	16.520	16.472	16.673	25.935	25.891	25.866	26.042
	0.17	17.464	17.411	17.365	17.591	27.538	27.488	27.470	27.678
$n = 4$	0.11	16.656	16.651	16.640	16.681	25.884	25.881	25.876	25.915
	0.14	17.322	17.310	17.307	17.352	26.528	26.519	26.432	26.569
	0.17	18.264	18.259	18.255	18.305	28.186	28.174	28.166	28.255

Table 5 Fundamental nondimensional frequency ($\bar{\omega} = \omega(b^2/h)\sqrt{\rho^m/E^m}$) of cross-ply $(0^C/90^F)_n$ hybrid laminated composite plates with various values of plate width-to-thickness ratio ($a/b = 1, f_{\text{CNT}}^* = 0.11$)

	b/h	SSSS				CCCC			
		[UD - F] _n	[Λ - F] _n	[O - F] _n	[X - F] _n	[UD - F] _n	[Λ - F] _n	[O - F] _n	[X - F] _n
$n = 1$	10	11.442	11.384	10.796	12.027	20.511	20.393	19.520	21.295
	20	12.230	12.163	11.491	12.925	24.847	24.651	23.311	26.210
	50	12.491	12.421	11.720	13.225	26.719	26.485	24.924	28.397
$n = 2$	10	15.939	15.874	15.853	16.032	25.292	25.266	25.211	25.392
	20	18.030	17.972	17.919	18.146	34.872	34.760	34.682	35.076
	50	18.820	18.786	18.699	18.945	40.568	40.477	40.301	40.842
$n = 4$	10	16.656	16.651	16.640	16.681	25.884	25.881	25.876	25.915
	20	19.112	19.103	19.089	19.141	36.483	36.470	36.448	36.537
	50	20.075	20.064	20.048	20.105	43.198	43.163	43.139	43.265

Table 6 Fundamental nondimensional frequency ($\bar{\omega} = \omega(b^2/h)\sqrt{\rho^m/E^m}$) of cross-ply $(0^C/90^F)_n$ hybrid laminated composite plates with various values of plate aspect ratio ($b/h = 10, f_{\text{CNT}}^* = 0.11$)

	a/b	SSSS				CCCC			
		[UD - F] _n	[Λ - F] _n	[O - F] _n	[X - F] _n	[UD - F] _n	[Λ - F] _n	[O - F] _n	[X - F] _n
$n = 1$	1.0	11.442	11.384	10.796	12.027	20.511	20.393	19.520	21.295
	1.5	8.856	8.783	8.676	9.036	16.171	16.005	15.801	16.510
	2.0	8.205	8.191	8.143	8.276	15.022	14.936	14.876	15.174
$n = 2$	1.0	15.939	15.874	15.853	16.032	25.292	25.266	25.211	25.392
	1.5	12.855	12.840	12.830	12.887	20.417	20.381	20.378	20.473
	2.0	11.923	11.923	11.921	11.925	18.979	18.966	18.965	19.011
$n = 4$	1.0	16.656	16.651	16.640	16.681	25.884	25.881	25.876	25.915
	1.5	13.485	13.483	13.480	13.495	20.931	20.931	20.930	20.952
	2.0	11.918	11.918	11.917	11.920	19.459	19.449	19.443	19.454

7080.0GPa, $G_{22}^{\text{CNT}} = 1944.5\text{GPa}$, $\nu_{12}^{\text{CNT}} = 0.175$, $\rho^{\text{CNT}} = 1400\text{kg/m}^3$. The CNTs efficiency parameters corresponding to the CNT volume fraction ($=0.11, 0.14$, and 0.17) are $\eta_1 = 0.149, \eta_2 = 0.934, \eta_3 = 0.934$, for the case of $f_{\text{CNT}}^* = 0.11$, and $\eta_1 = 0.150, \eta_2 = 0.941, \eta_3 = 0.941$, for the case of $f_{\text{CNT}}^* = 0.14$, and $\eta_1 = 0.149, \eta_2 = 1.381, \eta_3 = 1.381$, for the case of $f_{\text{CNT}}^* = 0.17$. It is assumed that $G_{12} = G_{13} = G_{23}$ for the plies made with CNTRC. Meanwhile, the graphite fibers are selected to be the reinforcement phase for the GFRC plies, whose properties are: $E_{11}^F = 233.05\text{GPa}$, $E_{22}^F = 23.1\text{GPa}$, $G_{12}^F = 8.96\text{GPa}$, $\nu^F = 0.2$, $\rho^F = 1750\text{kg/m}^3$. It is assumed that $G_{12} = G_{13}$ and $G_{23} = 1.2G_{12}$ for the plies made with GFRC. The volume fraction of the graphite fibers and the polymer matrix is, respectively, 0.6 and 0.4. In the following numerical applications, the i th nondimensional frequency parameter is given by [38]

$$\bar{\omega} = \omega(b^2/h)\sqrt{\rho^m/E^m} \quad (36)$$

Table 7 Fundamental nondimensional frequency ($\bar{\omega} = \omega(b^2/h)\sqrt{\rho^m/E^m}$) of angle-ply $(45^C/-45^F)_n$ hybrid laminated composite plates with various values of CNT volume fraction ($a/b = 1, b/h = 10$)

	f_{CNT}^*	SSSS				CCCC			
		[UD - F] _n	[Λ - F] _n	[O - F] _n	[X - F] _n	[UD - F] _n	[Λ - F] _n	[O - F] _n	[X - F] _n
$n = 1$	0.11	17.179	16.785	16.411	17.786	19.544	19.458	18.630	20.265
	0.14	17.702	17.089	16.819	18.382	20.022	19.836	18.984	20.819
	0.17	18.693	18.136	17.685	19.476	21.228	20.971	20.044	22.150
$n = 2$	0.11	22.307	22.291	22.232	22.396	24.242	24.193	24.161	24.341
	0.14	23.005	22.987	22.936	23.101	24.879	24.849	24.807	24.985
	0.17	24.345	24.304	24.288	24.467	26.393	26.375	26.338	26.530
$n = 4$	0.11	23.199	23.195	23.190	23.226	24.859	24.856	24.843	24.882
	0.14	23.903	23.902	23.900	23.938	25.497	25.494	25.491	25.536
	0.17	25.369	25.368	25.355	25.379	27.064	27.046	27.039	27.130

Table 8 Fundamental nondimensional frequency ($\bar{\omega} = \omega(b^2/h)\sqrt{\rho^m/E^m}$) of angle-ply $(45^C/-45^F)_n$ hybrid laminated composite plates with various values of plate width-to-thickness ratio ($a/b = 1, f_{\text{CNT}}^* = 0.11$)

	b/h	SSSS				CCCC			
		[UD - F] _n	[Λ - F] _n	[O - F] _n	[X - F] _n	[UD - F] _n	[Λ - F] _n	[O - F] _n	[X - F] _n
$n = 1$	10	17.179	16.785	16.411	17.786	19.544	19.458	18.630	20.265
	20	19.706	19.075	18.649	20.580	23.708	23.548	22.256	24.931
	50	20.702	20.024	19.519	21.697	25.748	25.538	23.970	27.292
$n = 2$	10	22.307	22.291	22.232	22.396	24.242	24.193	24.161	24.341
	20	28.373	28.347	28.230	28.523	32.962	32.857	32.781	33.155
	50	31.402	31.328	31.217	31.588	38.638	38.643	38.368	38.912
$n = 4$	10	23.199	23.195	23.190	23.226	24.859	24.856	24.843	24.882
	20	30.266	30.236	30.230	30.306	34.472	34.460	34.438	34.523
	50	34.048	34.015	34.006	34.094	41.074	41.049	41.015	41.141

Table 9 Fundamental nondimensional frequency ($\bar{\omega} = \omega(b^2/h)\sqrt{\rho^m/E^m}$) of angle-ply $(45^0/-45^0)_n$ hybrid laminated composite plates with various values of plate aspect ratio ($b/h = 10, f_{\text{CNT}}^* = 0.11$)

	a/b	SSSS				CCCC			
		[UD - F] _n	[Λ - F] _n	[O - F] _n	[X - F] _n	[UD - F] _n	[Λ - F] _n	[O - F] _n	[X - F] _n
$n = 1$	1.0	17.179	16.785	16.411	17.786	19.544	19.458	18.630	20.265
	1.5	12.620	12.242	12.011	13.106	15.193	15.119	14.434	15.807
	2.0	10.800	10.503	10.283	11.216	13.715	13.649	13.025	14.283
$n = 2$	1.0	22.307	22.291	22.232	22.396	24.242	24.193	24.161	24.341
	1.5	16.933	16.910	16.866	17.008	19.343	19.295	19.269	19.430
	2.0	14.669	14.623	14.609	14.735	17.607	17.575	17.538	17.688
$n = 4$	1.0	23.199	23.195	23.190	23.226	24.859	24.856	24.843	24.882
	1.5	16.192	16.184	16.175	16.219	19.913	19.907	19.900	19.921
	2.0	13.919	13.912	13.904	13.943	15.484	15.476	15.444	15.572

It should be noted that the power-law index P_{in} is taken to be 1.0 in the current paper unless otherwise specified.

4.1 Comparison studies

For the purpose of evaluating the accuracy and the reliability of the present approach, three test examples are performed. All of them are tested for the free vibration of composite plate structure.

The fundamental nondimensional frequency ($\bar{\omega} = \omega\sqrt{\rho_c/E_c}$) of square SSSS functionally graded material (FGM) plate is compared in Table 1 with the results reported by Matsunaga [55] through the higher-order shear deformation theory and by Song et al. [56] employing the FSDT. The results are compared with respect to different width-to-thickness ratio b/h , power-law index P_{in} , and mesh division. The constituent materials of the FGM plate are ceramic AL_2O_3 (c) and metal AL (m), whose properties are:

Table 10 First six nondimensional frequency ($\bar{\omega} = \omega(b^2/h)\sqrt{\rho^m/E^m}$) of cross-ply ($0^0/90^0$) hybrid laminated composite plates with various plate configuration ($a/b = 1, b/h = 10, \text{ and } f_{\text{CNT}}^* = 0.11$)

BCs	Plates configuration	Modes					
		1	2	3	4	5	6
SSSS	[Λ -F-V]	15.695	22.503	22.517	23.176	38.257	38.501
	[X-F-X-F]	16.032	23.654	23.686	35.233	35.816	45.589
	[Λ -F-V-F]	16.615	23.654	23.686	36.084	36.777	45.590
	[Λ -F-X-F-V]	16.540	22.957	22.982	32.101	38.454	44.410
	[Λ -F- Λ -F-V-F-V]	16.775	23.139	23.168	34.020	38.183	44.550
	[X-F-X-F-X-F-X-F]	16.681	23.608	23.646	35.987	36.686	45.194
	[Λ -F- Λ -F-V-F-V-F]	16.979	23.609	23.646	36.778	36.832	45.195
	[Λ -F-V]	22.089	30.921	40.737	45.497	46.346	56.338
CCCC	[X-F-X-F]	25.392	41.179	41.929	52.476	61.100	61.474
	[Λ -F-V-F]	25.730	41.505	42.862	53.190	61.106	61.693
	[Λ -F-X-F-V]	25.091	38.791	42.588	51.283	57.573	58.975
	[Λ -F- Λ -F-V-F-V]	25.671	40.115	42.873	52.191	59.419	59.607
	[X-F-X-F-X-F-X-F]	25.915	41.765	42.372	52.932	61.104	62.069
	[Λ -F- Λ -F-V-F-V-F]	26.187	41.935	42.850	53.305	61.107	62.193

Table 11 First six nondimensional frequency ($\bar{\omega} = \omega(b^2/h)\sqrt{\rho^m/E^m}$) of angle-ply ($45^0/-45^0$) hybrid laminated composite plates with various plate configuration ($a/b = 1, b/h = 10 \text{ and } f_{\text{CNT}}^* = 0.11$)

BCs	Plates configuration	Modes					
		1	2	3	4	5	6
SSSS	[Λ -F-V]	19.189	28.390	30.527	36.009	42.279	49.214
	[X-F-X-F]	22.396	31.540	36.837	37.037	54.441	55.990
	[Λ -F-V-F]	22.893	31.612	37.542	37.962	55.152	56.982
	[Λ -F-X-F-V]	22.350	30.892	35.073	38.202	52.292	55.218
	[Λ -F- Λ -F-V-F-V]	22.994	30.972	36.313	38.350	53.912	56.077
	[X-F-X-F-X-F-X-F]	23.226	31.300	37.460	37.838	55.238	56.511
	[Λ -F- Λ -F-V-F-V-F]	23.479	31.338	38.032	38.091	55.618	57.021
	[Λ -F-V]	20.902	31.945	37.790	43.813	51.392	55.639
CCCC	[X-F-X-F]	24.341	40.955	40.973	55.431	59.879	61.087
	[Λ -F-V-F]	24.880	41.435	41.856	56.108	60.604	61.091
	[Λ -F-X-F-V]	24.050	38.936	41.267	53.324	58.287	58.968
	[Λ -F- Λ -F-V-F-V]	24.628	40.205	41.744	54.778	59.341	59.597
	[X-F-X-F-X-F-X-F]	24.882	41.468	41.622	56.038	60.305	61.091
	[Λ -F- Λ -F-V-F-V-F]	25.157	41.861	41.933	56.400	60.693	61.093

$$E_c = 380.0\text{Gpa}, \nu_c = 0.3, \rho_c = 3800\text{kg/m}^3.$$

$$E_m = 70.0\text{Gpa}, \nu_m = 0.3, \rho_m = 2702\text{kg/m}^3.$$

The elastic modulus and the Poisson's ratio of the FGM plate are estimated using a layer-wise formulation, given as follows [50]:

$$E^{(k)} = (E_c - E_m) \left(\frac{k - 0.5}{N_L} \right)^{P_{in}} + E_m \tag{37}$$

$$\rho^{(k)} = (\rho_c - \rho_m) \left(\frac{k - 0.5}{N_L} \right)^{P_{in}} + \rho_m \tag{38}$$

$$\nu^{(k)} = 0.3 \tag{39}$$

where N_L is the total number of plate layers and $k = 1, 2, 3 \dots N_L$

It is observed that the present numerical results are in good agreement with those of the literature. Besides, the 8×8 mesh has produced reasonably converted results. Therefore, for all the following numerical results, the mesh size of 8×8 is used.

Table 2 compares the first six nondimensional frequency parameters of square cross-ply ($0^0/90^0/0^0/90^0/0^0$) CNTRC laminated plates with the results reported by Lei et al. [38]. Two kinds of boundary conditions which are all edges are simply supported (SSSS) or all edges are clamped (CCCC) and four CNT distribution patterns

Table 12 First six nondimensional frequency ($\bar{\omega} = \omega(b^2/h)\sqrt{\rho^m/E^m}$) of cross-ply ($0^0/90^0$) CNTRC laminated composite plates with various plate configuration ($a/b = 1$, $b/h = 50$, and $f_{CNT}^* = 0.11$)

BCs	Plates configuration	Modes					
		1	2	3	4	5	6
SSSS	[\Lambda-V]	10.425	29.301	29.353	41.145	63.382	63.672
	[V-\Lambda]	9.721	26.981	27.005	38.439	58.134	58.271
	[X-X]	13.092	36.911	36.958	51.394	79.461	79.714
	[\Lambda - \Lambda-V-V]	19.912	55.691	55.738	76.508	97.336	97.336
	[V-V-\Lambda - \Lambda]	15.124	42.557	42.597	58.986	90.938	91.140
	[X-X-X-X]	17.985	50.482	50.527	69.550	97.334	97.334
	[\Lambda - \Lambda - \Lambda - \Lambda-V-V-V-V]	20.005	55.881	55.908	76.736	97.324	97.324
	[V-V-V-V-\Lambda - \Lambda - \Lambda - \Lambda]	17.789	49.915	49.940	68.773	97.324	97.324
	[X-X-X-X-X-X-X-X-X]	18.995	53.194	53.220	73.148	97.322	97.322
CCCC	[\Lambda-V]	22.442	46.229	46.326	62.015	90.403	91.004
	[V-\Lambda]	20.544	42.417	42.463	57.386	83.260	83.604
	[X-X]	28.264	57.745	57.829	76.981	111.198	111.684
	[\Lambda - \Lambda-V-V]	42.495	84.213	84.282	111.008	153.888	154.211
	[V-V-\Lambda - \Lambda]	32.567	65.978	66.045	87.603	125.113	125.488
	[X-X-X-X]	38.581	77.173	77.242	101.988	143.185	143.532
	[\Lambda - \Lambda - \Lambda - \Lambda-V-V-V-V]	42.641	84.448	84.488	111.256	154.152	154.370
	[V-V-V-V-\Lambda - \Lambda - \Lambda - \Lambda]	38.155	76.372	76.412	100.910	141.845	142.080
	[X-X-X-X-X-X-X-X-X]	40.626	80.852	80.892	106.653	148.755	148.981

Table 13 First six nondimensional frequency ($\bar{\omega} = \omega(b^2/h)\sqrt{\rho^m/E^m}$) of angle-ply ($45^0/-45^0$) CNTRC laminated plates with various plate configuration ($a/b = 1$, $b/h = 50$ and $f_{CNT}^* = 0.11$)

BCs	Plates configuration	Modes					
		1	2	3	4	5	6
SSSS	[\Lambda-V]	17.826	32.836	32.931	58.929	59.960	66.261
	[V-\Lambda]	16.577	30.241	30.289	54.546	55.256	62.084
	[X-X]	21.451	40.897	40.968	73.349	73.387	79.918
	[\Lambda - \Lambda-V-V]	32.531	61.510	61.564	107.577	107.691	116.067
	[V-V-\Lambda - \Lambda]	26.142	47.770	47.821	84.141	86.059	94.293
	[X-X-X-X]	30.024	56.066	56.119	98.414	99.309	107.607
	[\Lambda - \Lambda - \Lambda - \Lambda-V-V-V-V]	33.605	62.086	62.117	107.940	109.233	118.312
	[V-V-V-V-\Lambda - \Lambda - \Lambda - \Lambda]	30.663	55.900	55.930	97.485	99.635	108.652
	[X-X-X-X-X-X-X-X-X]	32.286	59.301	59.332	103.260	104.954	114.003
CCCC	[\Lambda-V]	21.586	43.240	43.286	67.888	78.451	79.063
	[V-\Lambda]	19.849	39.926	39.948	62.333	73.053	73.607
	[X-X]	27.062	53.849	53.890	84.087	96.511	97.373
	[\Lambda - \Lambda-V-V]	40.313	78.534	78.571	119.985	135.870	137.478
	[V-V-\Lambda - \Lambda]	31.094	61.487	61.520	95.372	108.987	110.058
	[X-X-X-X]	36.684	71.905	71.941	110.581	125.621	127.010
	[\Lambda - \Lambda - \Lambda - \Lambda-V-V-V-V]	40.450	78.756	78.778	120.224	136.082	137.700
	[V-V-V-V-\Lambda - \Lambda - \Lambda - \Lambda]	36.555	71.522	71.785	110.123	125.091	126.479
	[X-X-X-X-X-X-X-X-X]	38.583	75.361	75.383	115.438	130.873	132.376

(FG-O, FG-V, UD, and FG-X) are considered in this comparison. In the modeling, the CNT volume fraction and width-to-thickness ratio are selected to be, respectively, 0.11 and 10. The present paper used the same theory used by Lei et al. [38] which is the FSDT, which in turn led to a good agreement between our results and those reported by Lei et al. [38].

The last comparison test concerns the nondimensional fundamental frequency parameter of square simply supported CNTRC laminated plates. The achieved results are compared in Table 3 with the results of Huang et al. [45]. In the analysis, the CNT volume fraction and width-to-thickness ratio are selected to be, respectively, 0.11 and 10. Three levels of the number of layers ($n = 1, 2$, and 4) and two kinds of stacking sequences which are cross-ply ($0^0/90^0$) and angle-ply ($45^0/-45^0$) are considered. As can be seen from Table 3, the obtained results are in good agreement with those of Huang et al. [45] for all four CNTs distribution patterns (FG-O, FG-V, UD, and FG-X).

Table 14 Fundamental nondimensional frequency ($\bar{\omega} = \omega(b^2/h)\sqrt{\rho^m/E^m}$) of cross-ply ($0^C/90^F/0^C/90^F$) hybrid laminated composite plates with various values of power-law index and CNT volume fraction ($a/b = 1, b/h = 10$)

BCs	f_{CNT}^*	Plates configuration	P_{in}					
			0.0	0.4	0.8	1.0	1.4	1.8
SSSS	0.11	[X-F-X-F]	15.939	15.988	16.018	16.032	16.055	16.075
		[Λ-F-V-F]	15.939	16.275	16.512	16.606	16.763	16.887
	0.14	[X-F-X-F]	16.566	16.622	16.657	16.673	16.700	16.726
		[Λ-F-V-F]	16.566	16.937	17.201	17.306	17.480	17.618
	0.17	[X-F-X-F]	17.464	17.529	17.572	17.591	17.629	17.664
		[Λ-F-V-F]	17.464	17.911	18.210	18.331	18.531	18.694
CCCC	0.11	[X-F-X-F]	25.292	25.343	25.375	25.392	25.418	25.443
		[Λ-F-V-F]	25.292	25.543	25.757	25.840	25.975	26.080
	0.14	[X-F-X-F]	25.935	25.988	26.025	26.042	26.076	26.109
		[Λ-F-V-F]	25.935	26.169	26.378	26.460	26.594	26.703
	0.17	[X-F-X-F]	27.538	27.602	27.652	27.678	27.728	27.782
		[Λ-F-V-F]	27.538	27.919	28.158	28.255	28.420	28.561

Table 15 Fundamental nondimensional frequency ($\bar{\omega} = \omega(b^2/h)\sqrt{\rho^m/E^m}$) of angle-ply ($45^C/-45^F/45^C/-45^F$) hybrid laminated composite plates with various values of power-law index and CNT volume fraction ($a/b = 1, b/h = 10$)

BCs	f_{CNT}^*	Plates configuration	P_{in}					
			0.0	0.4	0.8	1.0	1.4	1.8
SSSS	0.11	[X-F-X-F]	22.307	22.355	22.382	22.396	22.418	22.439
		[Λ-F-V-F]	22.307	22.578	22.776	22.854	22.980	23.080
	0.14	[X-F-X-F]	23.005	23.054	23.086	23.101	23.129	23.156
		[Λ-F-V-F]	23.005	23.267	23.468	23.548	23.678	23.783
	0.17	[X-F-X-F]	24.345	24.404	24.447	24.467	24.512	24.557
		[Λ-F-V-F]	24.345	24.720	24.949	25.041	25.197	25.329
CCCC	0.11	[X-F-X-F]	24.242	24.293	24.325	24.341	24.367	24.391
		[Λ-F-V-F]	24.242	24.497	24.713	24.797	24.934	25.041
	0.14	[X-F-X-F]	24.879	24.923	24.968	24.985	25.019	25.051
		[Λ-F-V-F]	24.879	25.124	25.339	25.423	25.562	25.674
	0.17	[X-F-X-F]	26.393	26.457	26.508	26.530	26.585	26.639
		[Λ-F-V-F]	26.393	26.776	27.021	27.120	27.289	27.432

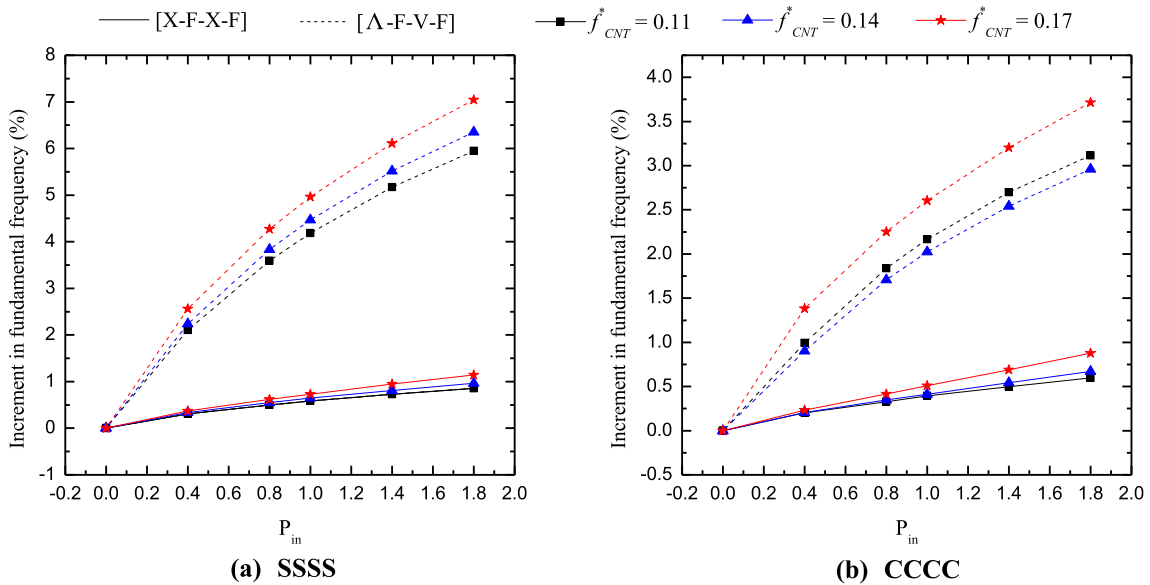


Fig. 4 The percentage increase in the fundamental frequency ($\Delta\bar{\omega} = 100 \times (\bar{\omega}_p - \bar{\omega}_u) / \bar{\omega}_u$) of cross-ply ($0^0/90^0/0^0/90^0$) hybrid laminated plate versus the power-law index P_{in} with different boundary conditions and plate configurations ($b/h = 10, a/b = 1.0$)

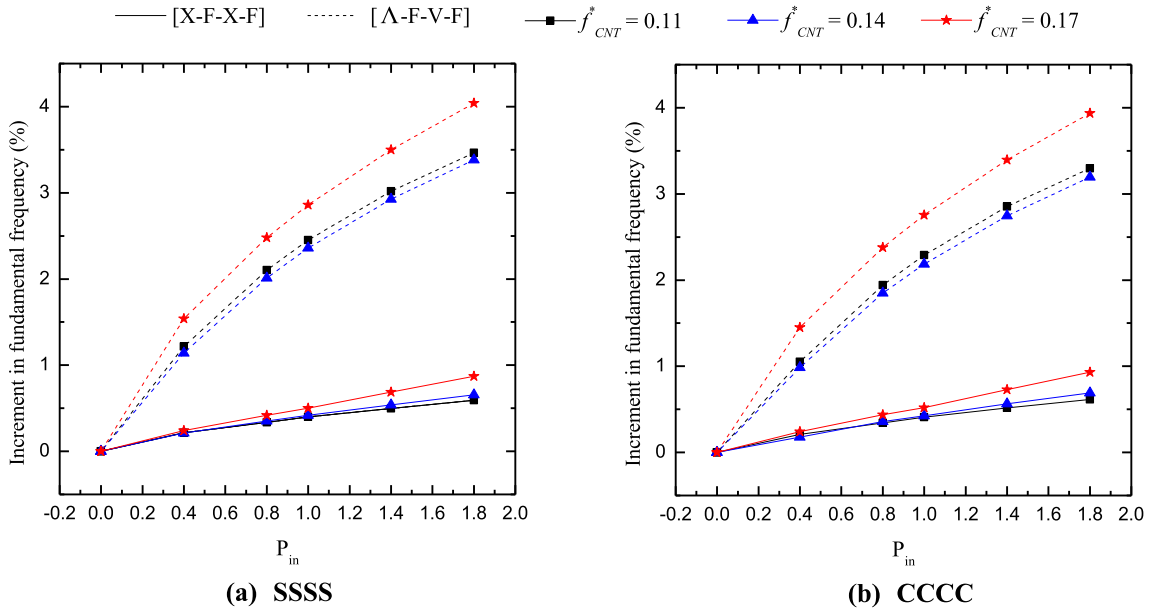


Fig. 5 The percentage increase in the fundamental frequency ($\Delta\bar{\omega} = 100 \times (\bar{\omega}_p - \bar{\omega}_u) / \bar{\omega}_u$) of angle-ply ($45^0 / -45^0 / 45^0 / -45^0$) hybrid laminated plate versus the power-law index P_{in} with different boundary conditions and plate configurations ($b/h = 10$, $a/b = 1.0$)

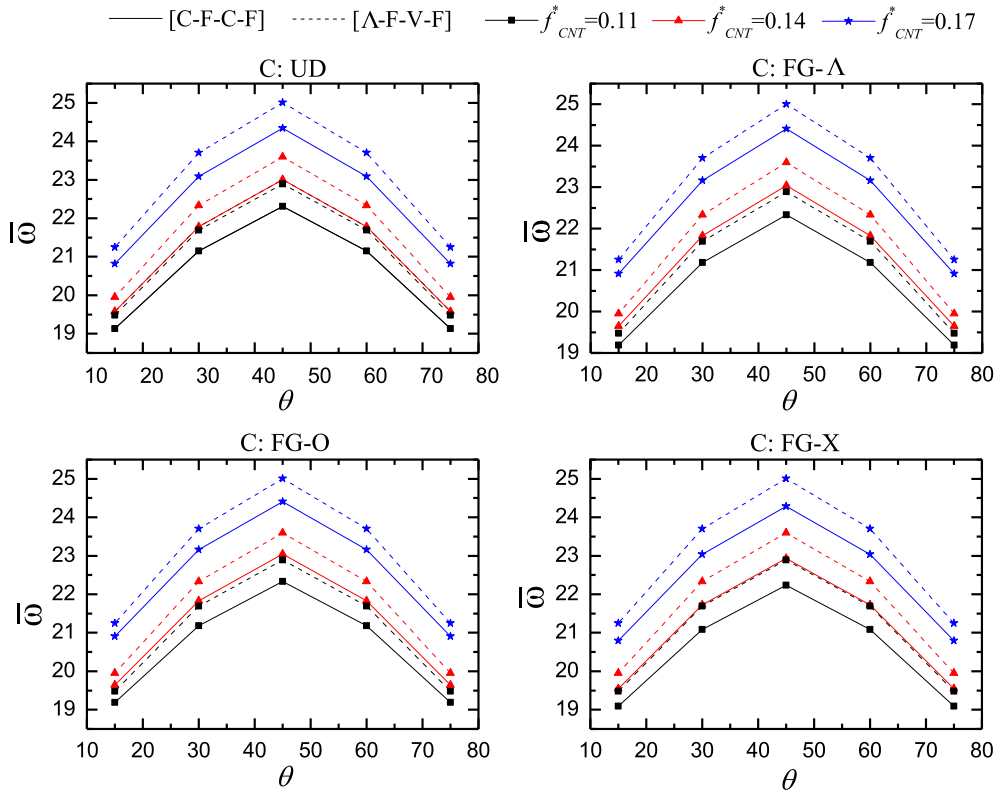


Fig. 6 Effect of orientation angle θ on the fundamental frequency $\bar{\omega} = \omega(b^2/h)\sqrt{\rho^m/E^m}$ of SSSS angle-ply ($\theta / -\theta / \theta / -\theta$) hybrid laminate plates with different values of CNT volume fraction and plate configuration ($a/b = 1$ and $b/h = 10$)

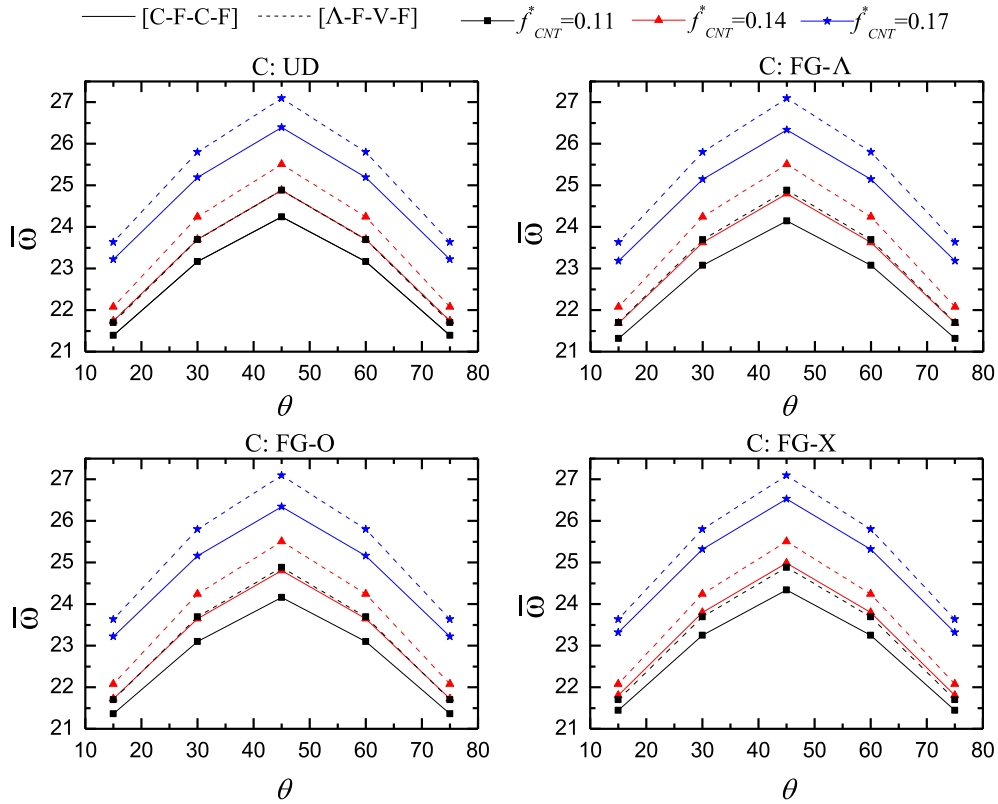


Fig. 7 Effect of orientation angle θ on the fundamental frequency $\bar{\omega} = \omega(b^2/h)\sqrt{\rho^m/E^m}$ of CCCC angle-ply ($\theta/ - \theta/ \theta/ - \theta$) hybrid laminate plates with different values of CNT volume fraction and plate configuration ($a/b = 1$ and $b/h = 10$)

4.2 Free vibration of hybrid laminated plates

Figure 3 shows the effect of number of ply' layers N_L on the fundamental nondimensional frequencies ($\bar{\omega}$) parameter of a single ply of CNTRC plate with different CNT distribution patterns. It can be observed that the $\bar{\omega}$ parameter of the plates with UD pattern is not affected by the increment of N_L , and the main physical reason for this circumstance is that the plates with UD pattern have a homogeneous distribution of CNT fillers. For the case where the CNTs are nonuniformly distributed, an increase in N_L leads to an increase in the $\bar{\omega}$ parameter for the plates with FG-X pattern and a decrease for the plates with FG- Λ and FG-O patterns. However, this trend is more obvious when N_L changes from 2 to 20; on the other hand, when $N_L > 20$, the fundamental nondimensional frequency parameter tends to converge to a constant value. Moreover, it is evident that the $\bar{\omega}$ parameter corresponding to FG- Λ pattern is least influenced by the variation of N_L among all three nonuniform distribution types. In the following numerical application, N_L is selected to be 20 layers ($N_L = 20$).

Tables 4, 5, and 6 present, respectively, the effect of volume fraction, width-to-thickness, and aspect ratios on the $\bar{\omega}$ parameter of cross-ply ($0^C/90^F$)_n hybrid laminated plates with different number of plies ($n = 1, 2,$ and 4), distribution types of CNTs (FG-O, FG- Λ , UD, and FG-X), and boundary condition (SSSS and CCCC). The superscripts C and F denote, respectively, the CNTRC and GFRC plies. Results indicate that under both SSSS and CCCC boundary conditions the $\bar{\omega}$ parameter increases with an increase in the CNT volume fraction (owing to the fact that the effective elastic properties of the CNT fillers are higher than the polymer matrix). In addition the $\bar{\omega}$ parameter increases and decreases, respectively, as the width-to-thickness ratio and aspect ratio increase. It can be also observed that the number of plies has a significant effect on the $\bar{\omega}$ parameter of the laminated plates, where the $\bar{\omega}$ parameter shows a rapid increase as the number of plies increases for all four CNT distribution patterns. Due to the fact that the FG-X pattern has much more CNTs near to both bottom and top surfaces, and that the FG-O pattern has much more CNTs near to the middle surface, the [X - F]_n and [O - F]_n configurations have, respectively, the largest and the smallest $\bar{\omega}$ parameter.

The fundamental nondimensional frequency $\bar{\omega}$ parameter of angle-ply ($45^C/ - 45^F$)_n hybrid laminated plates under the effects of CNT volume fraction, width-to-thickness ratio, and length-to-width ratio is, respec-

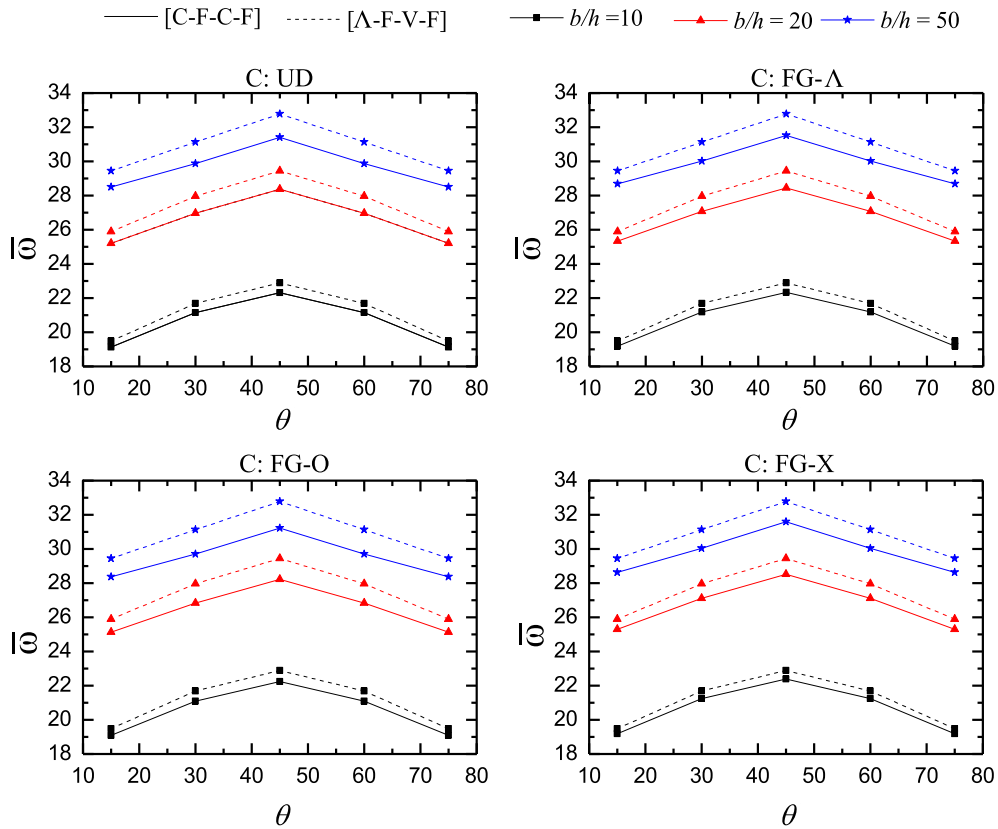


Fig. 8 Effect of orientation angle θ on the fundamental frequency $\bar{\omega} = \omega(b^2/h)\sqrt{\rho^m/E^m}$ of SSSS angle-ply ($\theta/ - \theta/ \theta/ - \theta$) hybrid laminate plates with different width-to-thickness ratio and plate configuration ($a/b = 1$ and $f_{CNT}^* = 0.11$)

tively, listed in Tables 7, 8, and 9. The influence of SSSS and CCCC boundary conditions and geometrical parameter including b/h ratio and a/b ratio on the $\bar{\omega}$ parameter is investigated. Similar observation to those obtained from the cross-ply hybrid laminated plates for CNT volume fraction, plies numbers, h/b and a/b ratios is found for both simply supported and clamped edges. For the same reasons mentioned in the previous case, the $[O - F]_n$ configuration has the smallest $\bar{\omega}$ parameter, while the $[X - F]_n$ configuration has the largest $\bar{\omega}$ parameter. It is also found that for all four CNT patterns and both stacking sequences, the $\bar{\omega}$ parameters corresponding to the plates with fully clamped edges are higher than those corresponding to the plates with fully simply supported edges.

Square hybrid laminated plates with different boundary conditions, number of layers, and laminate configuration (depending on different types of CNTs patterns) are investigated in this part. In the modeling, the CNT volume fraction and the width-to-thickness ratio are set to be 0.11 and 10, respectively. The first six nondimensional frequency $\bar{\omega}$ parameters of hybrid laminated plates are presented in Tables 10 and 11, respectively, for cross-ply and angle-ply staking sequences. It can be seen that all the first six $\bar{\omega}$ parameters corresponding to the laminated plate that containing the FG-V patterns in its upper half and the FG- Λ patterns in its lower half produce the highest frequency even higher than the plate that contains FG-X patterns; this is for both boundary conditions and cross-ply and angle-ply stacking sequences.

The combined influences of laminate configuration types, number of plies, and boundary condition on the first six nondimensional frequency $\bar{\omega}$ parameters of CNTRC laminated plates are examined in Tables 12 and 13, respectively, for cross-ply ($0^0/90^0/0^0/90^0$) and angle-ply ($45^0/ - 45^0/45^0/ - 45^0$) stacking sequences. In the analysis, the CNT volume fraction, b/h , and a/b are set to be 0.11, 10, and 1, respectively. From both Tables 12 and 13 results indicate that for ($n = 1$) the plates with $[X-X]$ configuration have the largest frequencies, while the plates with $[V - \Lambda]$ configuration yield the smallest frequencies in comparison with $[\Lambda - V]$ configuration, but for the case where $n=(4$ and $8)$ the laminated plate that contains each of FG-V and FG- Λ patterns, respectively, in the upper and lower half of the laminated plate provides the largest frequencies, which leads in turn to a high improvement in the stiffness of the plate, suggesting a laminated plate of four

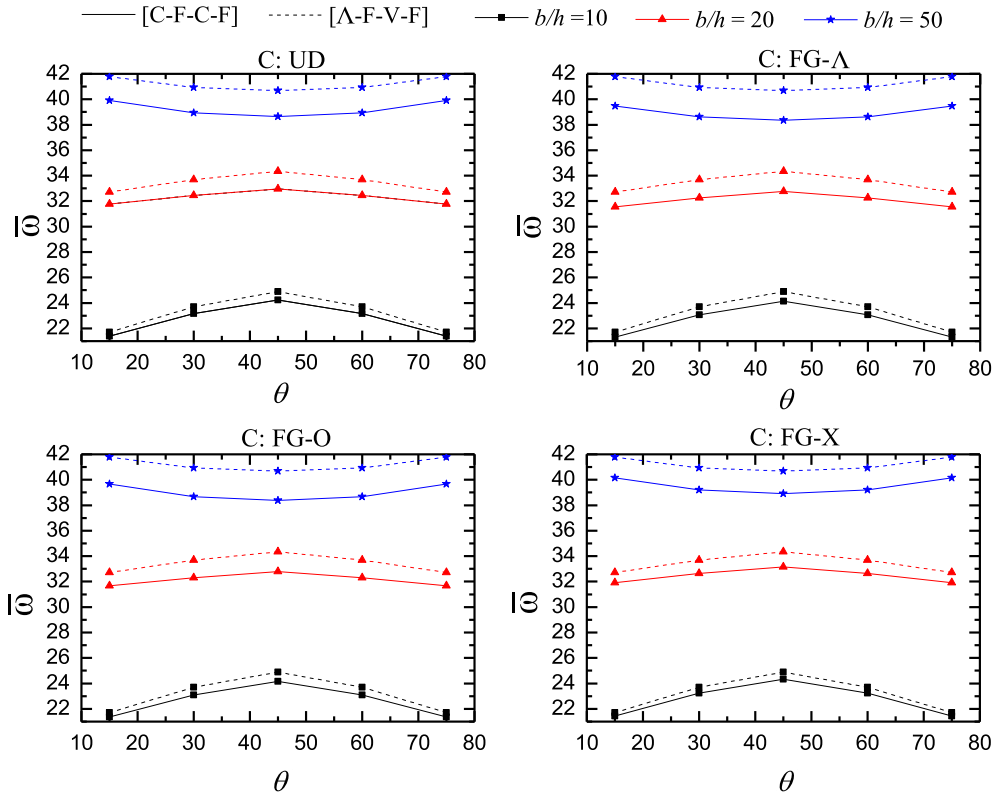


Fig. 9 Effect of orientation angle θ on the fundamental frequency $\bar{\omega} = \omega(b^2/h)\sqrt{\rho^m/E^m}$ of CCCC angle-ply ($\theta/ - \theta/ \theta/ - \theta$) hybrid laminate plates with different width-to-thickness ratio and plate configuration ($a/b = 1$ and $f_{CNT}^* = 0.11$)

or eight plies in which FG-V and FG-A patterns are putted-up, respectively, in its upper and lower half can provide the best structural performance for both SSSS and CCCC boundary conditions and cross-ply ($0^0/90^0$) and angle-ply ($45^0/ - 45^0$) stacking sequences.

Moreover, the combined effects of the power-law index, CNT volume fraction, and plate configuration on the nondimensional fundamental frequency $\bar{\omega}$ parameter of hybrid laminated plates are presented in Tables 14 and 15, respectively, for cross-ply ($0^0/90^0/0^0/90^0$) and angle-ply ($45^0/ - 45^0/45^0/ - 45^0$) staking sequences. Results indicate that an increase in the power-law index P_{in} leads to a higher $\bar{\omega}$ parameter for [X-F-X-F] and [Λ -F-V-F] laminated plate configurations. However, this phenomenon is more obvious with the [Λ -F-V-F] configuration where the corresponding $\bar{\omega}$ parameter rapidly increases with the increasing P_{in} . Thus, one can say that the plates with [Λ -F-V-F] configuration are more affected by P_{in} than those with [X-F-X-F] configuration. The same behavior is observed for both SSSS and CCCC boundary conditions, and cross-ply and angle-ply staking sequences. Again, these results indicate that the [Λ -F-V-F] configuration can provide plates with higher performance, especially if the CNT fillers are concentrate on the outer surfaces of each of FG- Λ and FG-V plies. For further explanations, Figs. 4 and 5 show the percentage increase in the nondimensional fundamental frequency ($\Delta\bar{\omega}$) verses the power-law index P_{in} , respectively, for cross-ply ($0^0/90^0/0^0/90^0$) and angle-ply ($45^0/ - 45^0/45^0/ - 45^0$) hybrid laminated plates with different CNT volume fraction. Herein, $\Delta\bar{\omega} = 100 \times (\bar{\omega}_p - \bar{\omega}_u) / \bar{\omega}_u$, where the $\bar{\omega}_u$ and $\bar{\omega}_p$ are, respectively, the nondimensional frequency with $P_{in}=0$ and $P_{in} \neq 0$. As can be seen, the largest variation in the percentage increase of the nondimensional fundamental frequency $\Delta\bar{\omega}$ is reached for higher values of CNT volume fraction. Besides, these results also provide an overview of the main advantage that the FG reinforcement can add to the field of nanocomposite materials, where the overall stiffness of the structure can tune by adjusting the distribution of the nanofillers across the ply thickness.

Figures 6 and 7 show the effect of CNT volume fraction and CNTs orientation angle θ on the $\bar{\omega}$ parameter of hybrid laminated plates under SSSS and CCCC boundary conditions, respectively. The width-to-thickness ratio and aspect ratio are set to be 10 and 1, respectively. As can be seen, the $\bar{\omega}$ parameter increases when the orientation angle θ varies from 15^0 to 45^0 , and decreases as the orientation angle θ varies from 45^0 to

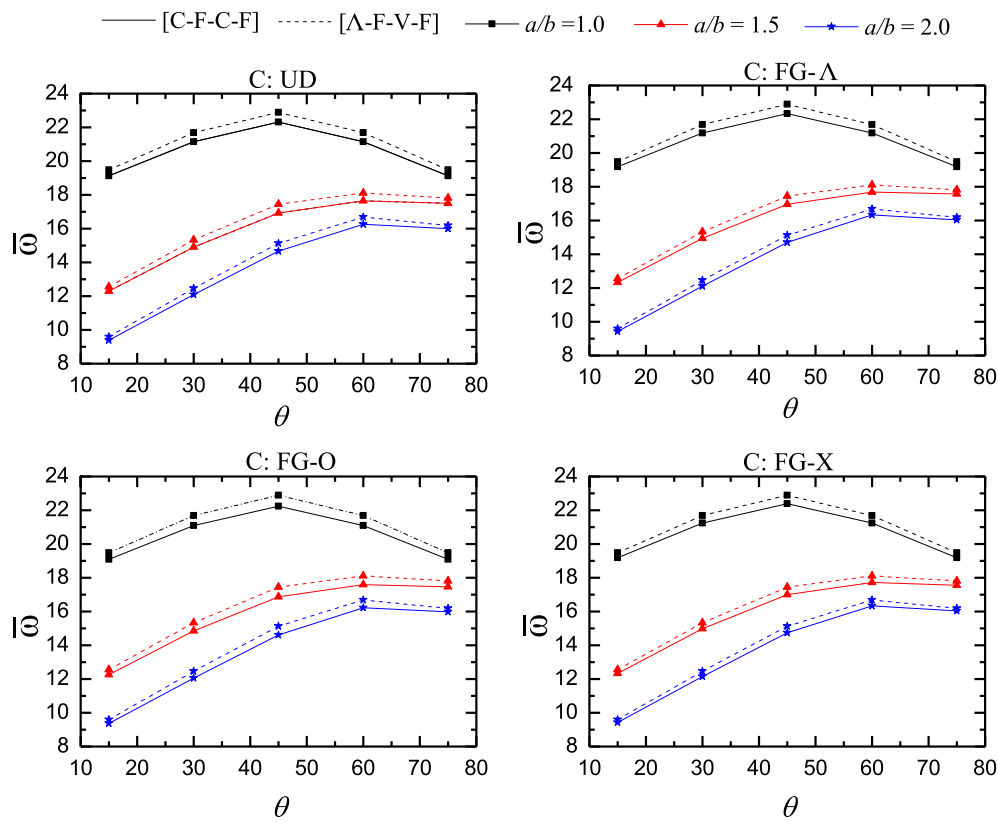


Fig. 10 Effect of orientation angle θ on the fundamental frequency $\bar{\omega} = \omega(b^2/h)\sqrt{\rho^m/E^m}$ of SSSS angle-ply ($\theta/ - \theta/ \theta/ - \theta$) hybrid laminate plates with different length-to-width ratio and plate configuration ($b/h = 10$ and $f_{CNT}^* = 0.11$)

75^0 . It can be also found that the $\bar{\omega}$ parameter is symmetric under the orientation angle $\theta = 45^0$ for all CNTs distribution patterns and SSSS and CCCC boundary conditions.

The effect of the width-to-thickness ratio together with the fillers orientation angle θ on the $\bar{\omega}$ parameter of hybrid laminated plates is illustrated in Figs. 8 and 9, respectively, for SSSS and CCCC boundary conditions. In the modeling, the plate aspect ratio and

CNT volume fraction are set to be 1 and 0.11, respectively. It is evident that the observation of the previous study can be sensed again, except the case corresponding to CCCC thin ($b/h = 50$) plate, where the $\bar{\omega}$ parameter decreases when the orientation angle θ varies from 15^0 to 45^0 , and increases as the orientation angle θ varies from 45^0 to 75^0 as depicted in Fig. 9.

Figures 10 and 11 give the variation of the $\bar{\omega}$ parameter of hybrid laminated plates due to the influence caused by different length-to-width ratio and the CNT fillers orientation angle θ for SSSS and CCCC boundary conditions, respectively. In the analysis, the width-to-thickness ratio and CNT volume fraction are set to be 10 and 0.11, respectively. The frequency curve corresponding to square plate ($a/b = 1$) is symmetric under the orientation angle $\theta = 45^0$, while the frequency curve corresponding to $a/b = 1.5$ and $a/b = 2.0$ keeps increasing when the orientation angle θ varies from 15^0 to 75^0 . It is also found from Figs. 6, 7, 8, 9, 10, and 11 that the $[\Lambda-F-V-F]$ configuration gained the largest values of $\bar{\omega}$ parameter for various width-to-thickness ratios, CNT volume fractions, aspect ratios, and two types of staking sequences and boundary conditions. Next, the first six three-dimensional mode shapes of angle-ply ($45^0/ - 45^0/45^0/ - 45^0$) hybrid laminated plate with width-to-thickness ratio of 10, CNTs volume fraction of 0.11, and $[\Lambda-F-V-F]$ configuration are illustrated in Figs. 12 and 13, respectively, for SSSS and CCCC boundary conditions.

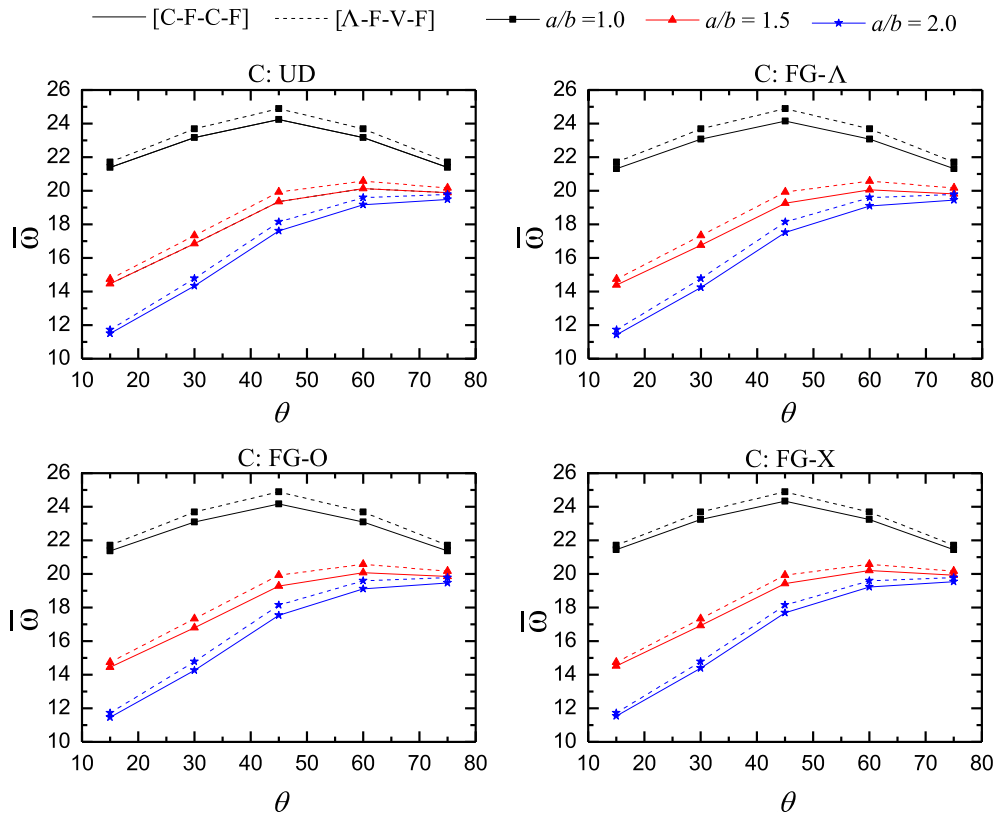


Fig. 11 Effect of orientation angle θ on the fundamental frequency $\bar{\omega} = \omega(b^2/h)\sqrt{\rho^m/E^m}$ of CCCC angle-ply ($\theta/\theta/\theta/\theta$) hybrid laminate plates with different length-to-width ratio and plate configuration ($b/h = 10$ and $f_{CNT}^* = 0.11$)

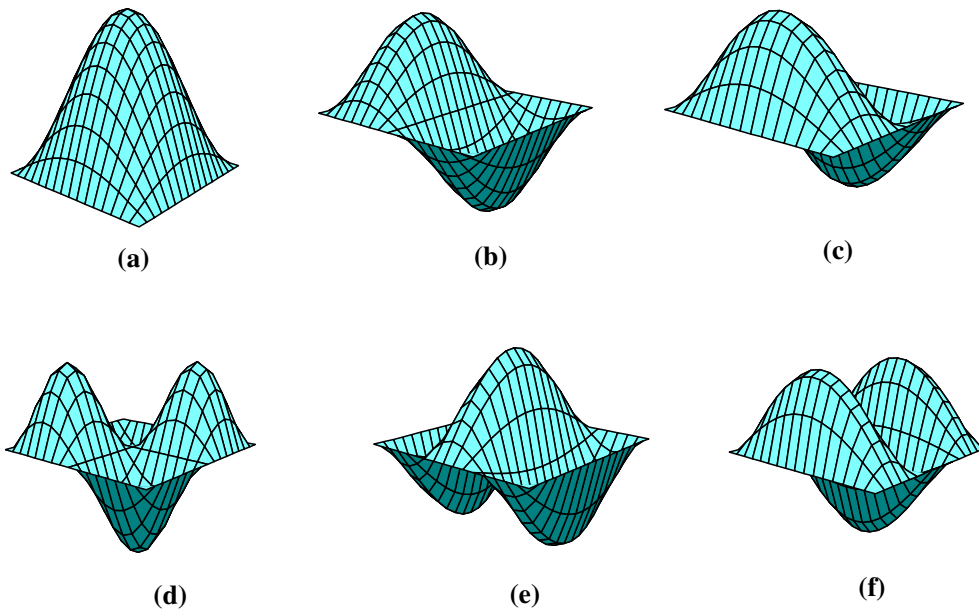


Fig. 12 The first six three-dimensional mode shapes of angle-ply ($45^0/45^0/45^0/45^0$) hybrid laminated plate with SSSS boundary condition and [Λ -F-V-F] configuration. **a** Mode 1, **b** Mode 2, **c** Mode 3, **d** Mode 4, **e** Mode 5, **f** Mode 6

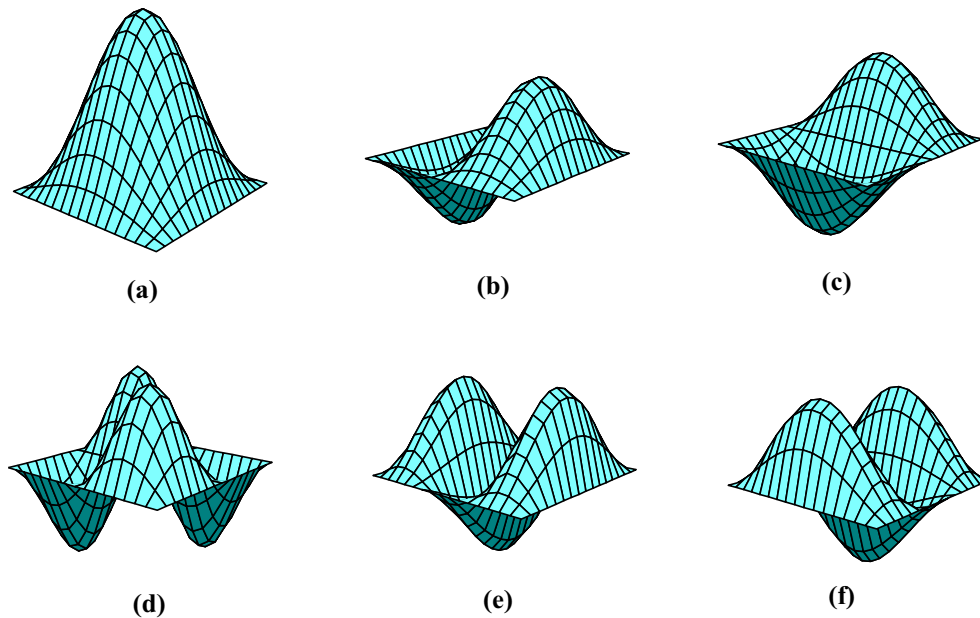


Fig. 13 The first six three-dimensional mode shapes of angle-ply ($45^0 / -45^0 / 45^0 / -45^0$) hybrid laminated plate with CCCC boundary condition and $[\Lambda\text{-F-V-F}]$ configuration. **a** Mode 1, **b** Mode 2, **c** Mode 3, **d** Mode 4, **e** Mode 5, **f** Mode 6

5 Conclusion

In order to enrich the existing research that investigates the mechanical behavior of laminated nanocomposite structures, this paper presents a study on free vibration behavior of hybrid laminated composite plates made with GFRC and CNTRC plies using a layer-wise formulation. The mechanical properties are determined by means of the extended rule of mixture micromechanics model. Self-made finite element code based on first-order shear deformation plate theory has been employed to carry out the numerical studies. Firstly, a comparison studies were performed to demonstrate the effectiveness and the accuracy of the present approach. Thereafter, focusing on the influence of different plate configuration and linear and nonlinear distribution of nanofillers, various numerical tests were conducted in order to investigate the effect of CNT distribution patterns, the number of CNTRC ply' layers, CNT volume fraction, geometrical parameter, number of plies, and boundary conditions. Overall, the main findings of the present study are outlined as follows:

- Results reveal that CNTRC plies that divided into 20 layers ($N_L = 20$) can provide sufficiently accurate results.
- Increases in the number of plies cause to increase the fundamental frequency of the hybrid laminated plates.
- It was discovered that the configuration of the laminated plate structures with special layout arrangement using the CNT distribution types can remarkably enhance its performance. For instance, the plates with configuration $[\Lambda\text{-F-V-F}]$ produced the highest fundamental frequency.
- It was also revealed that the accumulation of the CNT fillers on the outer surfaces of the FG- Λ and FG-V distribution patterns can lead to a large enhancement on the performance of the hybrid laminated plate that has $[\Lambda\text{-F-V-F}]$ configuration.
- Results show that the fundamental frequency increases as the orientation angle θ varies from 15^0 to 45^0 and decreases as the orientation angle θ varies from 45^0 to 75^0 for different values of CNTs volume fraction and width-to-thickness ratio, while keeps increasing for different values of the length-to-width ratio.
- A small increase in the CNT volume fraction can lead to a rapid and more remarkable variation in the fundamental frequency.
- The fundamental frequencies of the hybrid laminated structure increase and decrease, respectively, as the width-to-thickness and the length-to-width ratios of the plate increase.
- The fundamental frequency of the hybrid laminated strongly depends on the boundary conditions case, where the plates with clamped edges produce the highest frequency compared to the plates that are simply supported.

Compliance with ethical standards

Conflict of interest On behalf of all authors, the corresponding author states that there is no conflict of interest.

References

1. Esawi, A.M.K., Farag, M.M.: Carbon nanotube reinforced composites: potential and current challenges. *Mater. Des.* **28**, 2394–2401 (2007)
2. Han, Y., Elliott, J.: Molecular dynamics simulations of the elastic properties of polymer/carbon nanotube composites. *Comput. Mater. Sci.* **39**, 315–323 (2007)
3. Seidel, G.D., Lagoudas, D.C.: Micromechanical analysis of the effective elastic properties of carbon nanotube reinforced composites. *Mech. Mater.* **38**, 884–907 (2006)
4. Wuite, J., Adali, S.: Deflection and stress behaviour of nanocomposite reinforced beams using a multiscale analysis. *Compos. Struct.* **71**, 388–396 (2005)
5. Formica, G., Lacarbonara, W., Alessi, R.: Vibrations of carbon nanotube-reinforced composites. *J. Sound Vib.* **329**, 1875–1889 (2010)
6. Kim, M., Park, Y.-B., Okoli, O.I., Zhang, C.: Processing, characterization, and modeling of carbon nanotube-reinforced multiscale composites. *Compos. Sci. Technol.* **69**, 335–342 (2009)
7. Thostenson, E.T., Ren, Z., Chou, T.-W.: Advances in the science and technology of carbon nanotubes and their composites: a review. *Compos. Sci. Technol.* **61**, 1899–1912 (2001)
8. Thostenson, E.T., Li, W.Z., Wang, D.Z., Ren, Z.F., Chou, T.W.: Carbon nanotube/carbon fiber hybrid multiscale composites. *J. Appl. Phys.* **91**, 6034–6037 (2002)
9. Godara, A., Mezzo, L., Luizi, F., Warriar, A., Lomov, S.V., Van Vuure, A.W., Gorbatikh, L., Moldenaers, P., Verpoest, I.: Influence of carbon nanotube reinforcement on the processing and the mechanical behaviour of carbon fiber/epoxy composites. *Carbon N. Y.* **47**, 2914–2923 (2009)
10. Griebel, M., Hamaekers, J.: Molecular dynamics simulations of the elastic moduli of polymer-carbon nanotube composites. *Comput. Methods Appl. Mech. Eng.* **193**, 1773–1788 (2004)
11. Qian, D., Dickey, E.C., Andrews, R., Rantell, T.: Load transfer and deformation mechanisms in carbon nanotube-polystyrene composites. *Appl. Phys. Lett.* **76**, 2868–2870 (2000)
12. Liew, K.M., Pan, Z., Zhang, L.-W.: The recent progress of functionally graded CNT reinforced composites and structures. *Sci. CHINA Physics, Mech. Astron.* **63**, 234601 (2020)
13. Li, S.-R., Ma, H.-K.: Analysis of free vibration of functionally graded material micro-plates with thermoelastic damping. *Arch. Appl. Mech.* **1–20**
14. Thai, H.-T., Park, T., Choi, D.-H.: An efficient shear deformation theory for vibration of functionally graded plates. *Arch. Appl. Mech.* **83**, 137–149 (2013)
15. Fallah, A., Aghdam, M.M., Kargarnovin, M.H.: Free vibration analysis of moderately thick functionally graded plates on elastic foundation using the extended Kantorovich method. *Arch. Appl. Mech.* **83**, 177–191 (2013)
16. Shariyat, M., Alipour, M.M.: Differential transform vibration and modal stress analyses of circular plates made of two-directional functionally graded materials resting on elastic foundations. *Arch. Appl. Mech.* **81**, 1289–1306 (2011)
17. Ebrahimi, F., Rastgoo, A.: Nonlinear vibration analysis of piezo-thermo-electrically actuated functionally graded circular plates. *Arch. Appl. Mech.* **81**, 361–383 (2011)
18. Shen, H.-S.: Nonlinear bending of functionally graded carbon nanotube-reinforced composite plates in thermal environments. *Compos. Struct.* **91**, 9–19 (2009)
19. Zhu, P., Lei, Z.X., Liew, K.M.: Static and free vibration analyses of carbon nanotube-reinforced composite plates using finite element method with first order shear deformation plate theory. *Compos. Struct.* **94**, 1450–1460 (2012)
20. Ansari, R., Hasrati, E., Shojaei, M.F., Gholami, R., Shahabodini, A.: Forced vibration analysis of functionally graded carbon nanotube-reinforced composite plates using a numerical strategy. *Phys. E Low Dimens. Syst. Nanostruct.* **69**, 294–305 (2015)
21. Trabelssi, M., El-Borgi, S., Friswell, M.I.: A high-order FEM formulation for free and forced vibration analysis of a nonlocal nonlinear graded Timoshenko nanobeam based on the weak form quadrature element method. *Arch. Appl. Mech.* **1–24**, (2020)
22. Bouazza, M., Zenkour, A.M.: Vibration of carbon nanotube-reinforced plates via refined nth-higher-order theory. *Arch. Appl. Mech.* (2020)
23. Zhang, L.W., Cui, W.C., Liew, K.M.: Vibration analysis of functionally graded carbon nanotube reinforced composite thick plates with elastically restrained edges. *Int. J. Mech. Sci.* **103**, 9–21 (2015)
24. Zhang, L.W., Lei, Z.X., Liew, K.-M.: Computation of vibration solution for functionally graded carbon nanotube-reinforced composite thick plates resting on elastic foundations using the element-free IMLS-Ritz method. *Appl. Math. Comput.* **256**, 488–504 (2015)
25. Hieu, P.T., Van Tung, H.: Thermal and thermomechanical buckling of shear deformable FG-CNTRC cylindrical shells and toroidal shell segments with tangentially restrained edges. *Arch. Appl. Mech.* **1–18**, (2020)
26. Farzam, A., Hassani, B.: Thermal and mechanical buckling analysis of FG carbon nanotube reinforced composite plates using modified couple stress theory and isogeometric approach. *Compos. Struct.* **206**, 774–790 (2018)
27. Lei, Z.X., Liew, K.M., Yu, J.L.: Buckling analysis of functionally graded carbon nanotube-reinforced composite plates using the element-free kp-Ritz method. *Compos. Struct.* **98**, 160–168 (2013)
28. Zhang, L.W., Liew, K.M.: Postbuckling analysis of axially compressed CNT reinforced functionally graded composite plates resting on Pasternak foundations using an element-free approach. *Compos. Struct.* **138**, 40–51 (2016)

29. Zhang, L.W., Liew, K.M., Reddy, J.N.: Postbuckling of carbon nanotube reinforced functionally graded plates with edges elastically restrained against translation and rotation under axial compression. *Comput. Methods Appl. Mech. Eng.* **298**, 1–28 (2016)
30. Alibeigloo, A., Emtehani, A.: Static and free vibration analyses of carbon nanotube-reinforced composite plate using differential quadrature method. *Meccanica* **50**, 61–76 (2015)
31. Kiani, Y.: Free vibration of FG-CNT reinforced composite skew plates. *Aerosp. Sci. Technol.* **58**, 178–188 (2016)
32. Zhang, L.W.: On the study of the effect of in-plane forces on the frequency parameters of CNT-reinforced composite skew plates. *Compos. Struct.* **160**, 824–837 (2017)
33. Zhang, L.W., Lei, Z.X., Liew, K.M.: Free vibration analysis of functionally graded carbon nanotube-reinforced composite triangular plates using the FSDT and element-free IMLS-Ritz method. *Compos. Struct.* **120**, 189–199 (2015)
34. Zhang, L.W., Lei, Z.X., Liew, K.M.: Free vibration analysis of FG-CNT reinforced composite straight-sided quadrilateral plates resting on elastic foundations using the IMLS-Ritz method. *J. Vib. Control.* **23**, 1026–1043 (2017)
35. Ansari, R., Shahabodini, A., Shojaei, M.F.: Vibrational analysis of carbon nanotube-reinforced composite quadrilateral plates subjected to thermal environments using a weak formulation of elasticity. *Compos. Struct.* **139**, 167–187 (2016)
36. Fantuzzi, N., Tornabene, F., Baccocchi, M., Dimitri, R.: Free vibration analysis of arbitrarily shaped Functionally Graded Carbon Nanotube-reinforced plates. *Compos. Part B Eng.* **115**, 384–408 (2017)
37. Wang, Z.-X., Shen, H.-S.: Nonlinear vibration and bending of sandwich plates with nanotube-reinforced composite face sheets. *Compos. Part B Eng.* **43**, 411–421 (2012)
38. Lei, Z.X., Zhang, L.W., Liew, K.M.: Free vibration analysis of laminated FG-CNT reinforced composite rectangular plates using the kp-Ritz method. *Compos. Struct.* **127**, 245–259 (2015)
39. Lei, Z.X., Zhang, L.W., Liew, K.M.: Analysis of laminated CNT reinforced functionally graded plates using the element-free kp-Ritz method. *Compos. Part B Eng.* **84**, 211–221 (2016)
40. Lei, Z.X., Zhang, L.W., Liew, K.M.: Buckling analysis of CNT reinforced functionally graded laminated composite plates. *Compos. Struct.* **152**, 62–73 (2016)
41. Shen, H.-S., Xiang, Y.: Postbuckling behavior of functionally graded graphene-reinforced composite laminated cylindrical shells under axial compression in thermal environments. *Comput. Methods Appl. Mech. Eng.* **330**, 64–82 (2018)
42. Lei, Z.X., Zhang, L.W., Liew, K.M.: Parametric analysis of frequency of rotating laminated CNT reinforced functionally graded cylindrical panels. *Compos. Part B Eng.* **90**, 251–266 (2016)
43. Malekzadeh, P., Zarei, A.R.: Free vibration of quadrilateral laminated plates with carbon nanotube reinforced composite layers. *Thin-Walled Struct.* **82**, 221–232 (2014)
44. Malekzadeh, P., Heydarpour, Y.: Mixed Navier-layerwise differential quadrature three-dimensional static and free vibration analysis of functionally graded carbon nanotube reinforced composite laminated plates. *Meccanica*. **50**, 143–167 (2015)
45. Huang, B., Guo, Y., Wang, J., Du, J., Qian, Z., Ma, T., Yi, L.: Bending and free vibration analyses of antisymmetrically laminated carbon nanotube-reinforced functionally graded plates. *J. Compos. Mater.* **51**, 3111–3125 (2017)
46. Fan, Y., Wang, H.: Thermal postbuckling and vibration of postbuckled matrix cracked hybrid laminated plates containing carbon nanotube reinforced composite layers on elastic foundation. *Compos. Struct.* **157**, 386–397 (2016)
47. Lei, Z.X., Zhang, L.W., Liew, K.M.: Modeling large amplitude vibration of matrix cracked hybrid laminated plates containing CNTR-FG layers. *Appl. Math. Model.* **55**, 33–48 (2018)
48. Lei, Z.X., Yin, B.B., Liew, K.M.: Bending and vibration behaviors of matrix cracked hybrid laminated plates containing CNTR-FG layers and FRC layers. *Compos. Struct.* **184**, 314–326 (2018)
49. Pan, Z.Z., Zhang, L.W., Liew, K.M.: Modeling geometrically nonlinear large deformation behaviors of matrix cracked hybrid composite deep shells containing CNTRC layers. *Comput. Methods Appl. Mech. Eng.* **355**, 753–778 (2019)
50. Chiker, Y., Bachene, M., Guemana, M., Attaf, B., Rechak, S.: Free vibration analysis of multilayer functionally graded polymer nanocomposite plates reinforced with nonlinearly distributed carbon-based nanofillers using a layer-wise formulation model. *Aerosp. Sci. Technol.* **105913**, (2020)
51. Shen, H.-S.: A comparison of buckling and postbuckling behavior of FGM plates with piezoelectric fiber reinforced composite actuators. *Compos. Struct.* **91**, 375–384 (2009)
52. Fidelus, J.D., Wiesel, E., Gojny, F.H., Schulte, K., Wagner, H.D.: Thermo-mechanical properties of randomly oriented carbon/epoxy nanocomposites. *Compos. Part A Appl. Sci. Manuf.* **36**, 1555–1561 (2005)
53. Reddy, J.N.: *Mechanics of Laminated Composite Plates and Shells: Theory and Analysis*. CRC Press, Boca Raton (2003)
54. Huang, H.-C.: *Static and Dynamic Analyses of Plates and Shells: Theory, Software and Applications*. Springer, Berlin (2012)
55. Matsunaga, H.: Free vibration and stability of functionally graded plates according to a 2-D higher-order deformation theory. *Compos. Struct.* **82**, 499–512 (2008)
56. Song, M., Kitipornchai, S., Yang, J.: Free and forced vibrations of functionally graded polymer composite plates reinforced with graphene nanoplatelets. *Compos. Struct.* **159**, 579–588 (2017)